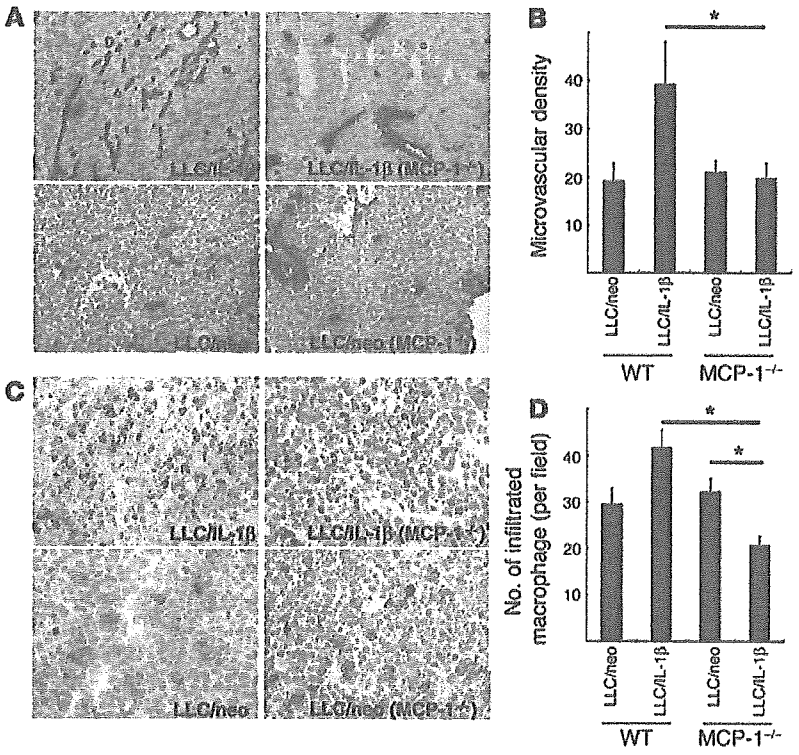

Figure 7
Enhancement of angiogenesis and macrophage infiltration by LLC/IL-1β was inhibited in MCP-1$^{-/-}$ mice (**A**) Representative photographs of CD31-stained sections from LLC tumors in wild-type or MCP-1$^{-/-}$ mice. Magnification, ×400. (**B**) CD31-positive microvascular densities obtained by morphometric analysis of LLC tumors. Each value represents the mean number of vessels ± SD in 5 fields. *P < 0.01 versus LLC/IL-1β. (**C**) Infiltration of macrophages stained with mAb F4/80 in LLC/neo and LLC/IL-1β tumors. Magnification, ×200. (**D**) Quantification of the number of macrophages infiltrating LLC/IL-1β and LLC/neo tumors. Magnification, ×400. Each value represents the mean number of macrophages ± SD in 5 microscopic fields. *P < 0.01 versus LLC/IL-1β in wild-type mice using the Mann-Whitney U test.

implantation (Figure 9, A–C). ENA-78 (CXCL5) mRNA levels were also increased in IL-1β–implanted corneas compared with controls (Figure 9D). Anti-mouse CXCR2 Ab inhibited IL-1β–implanted corneal angiogenesis by 32% (Figure 9, E and F).

CXC chemokines and VEGF-A are involved in COX-2–associated angiogenesis (37, 38). VEGF-A and KC levels were decreased in the IL-1β–implanted corneas of DFU-treated mice compared with control mice (Figure 9, G and H). ELR$^+$ CXC chemokine–CXCR2 signaling was therefore important for COX-2–related angiogenesis induced by IL-1β.

Discussion

IL-1 has been implicated in the growth of solid tumors, hematopoiesis, leukemia, and atherosclerosis (3). IL-1β is overexpressed in ovarian cancer cells in culture (39) and in patients with renal cell and gastric cancers (40, 41); it is essential for inflammatory and tumor-associated angiogenesis in animal models (6–8). Reduced angiogenesis and tumor enlargement have been reported in IL-1β–KO mice (8, 10). Various angiogenesis-related factors are upregulated by IL-1β overexpression when human lung cancer cells are transplanted into animals (7). Bar et al. reported that IL-1 receptor antagonist inhibited IL-1β–transfected tumor proliferation in an in vivo xenograft model (9).

Tumors expressing IL-1β are characterized by the infiltration of neutrophils, lymphocytes, and macrophages (9). However, it has been unclear which was most important in IL-1β–induced angiogenesis. We used 2 assays to confirm that IL-1β–induced angiogenesis was suppressed in mouse corneas by monocyte/macrophage depletion. First, Cl_2MDP-LIPs (i.v. and s.c.) blocked monocyte/macrophage infiltration and IL-1β–induced angiogenesis, depleting macrophages but not neutrophils or lymphocytes (33, 34). Second, neovascularization and the numbers of infiltrating macrophages were reduced in MCP-1$^{-/-}$ mice given IL-1β–containing corneal implants. MCP-1 acts potently on mononuclear cells, including monocytes and lymphocytes. MCP-1$^{-/-}$ mice have shown impaired macrophage recruitment in several inflammatory models in vivo (13–15). Neutrophil depletion by anti-Gr-1 mAb did not affect IL-1β–induced corneal angiogenesis. These results suggest that the infiltration of monocytes/macrophages rather than neutrophils is crucial in IL-1β–induced angiogenesis.

Conejo-Garcia et al. (42) reported that angiogenesis induced by infiltrating dendritic cell precursors was mediated through the cooperation of β-defensins and VEGF-A, suggesting the involvement of immune mechanisms in tumor angiogenesis (42). The role of dendritic cell infiltration in IL-1β–induced angiogenesis and the effect of Cl_2MDP-LIPs on dendritic cells have been unclear. Zhang et al. (43) reported that Cl_2MDP-LIPs depleted CD11c-positive dendritic cells in the spleen but not in peripheral blood. Cheng et al. (44) demonstrated that s.c. injection of Cl_2MDP-LIPs depleted macrophages but not dendritic cells. We found that CD11c$^+$ dendritic cells were 1.4% ± 0.5% (PBS-LIP treatment) and 1.3% ± 0.4% (Cl_2MDP-LIP treatment), respectively, of total cells in peripheral blood when Cl_2MDP-LIPs were administered both i.v. and s.c. (n = 5; Supplemental Figure S1; supplemental material available online with this article; doi:10.1172/JCI23298DS1). The numbers of infiltrating CD11c$^+$ dendritic cells in IL-1β–treated corneas were similar in Cl_2MDP-LIP– and PBS-LIP–treated mice (Supplemental Figure S2). IL-1β–induced angiogenesis was blocked in MCP-1$^{-/-}$ mice (Figure 3), and dendritic cells did not express the CCR2 cognate receptor for MCP-1. Thus, infiltrating dendritic cells are unlikely to be important in neovascularization mediated by IL-1β.

Maximum MCP-1 expression occurred 1 day after IL-1β implantation into mouse corneas (Figure 3). MCP-1 is essential in the recruitment of angiogenic macrophages (12, 16). In wild-type

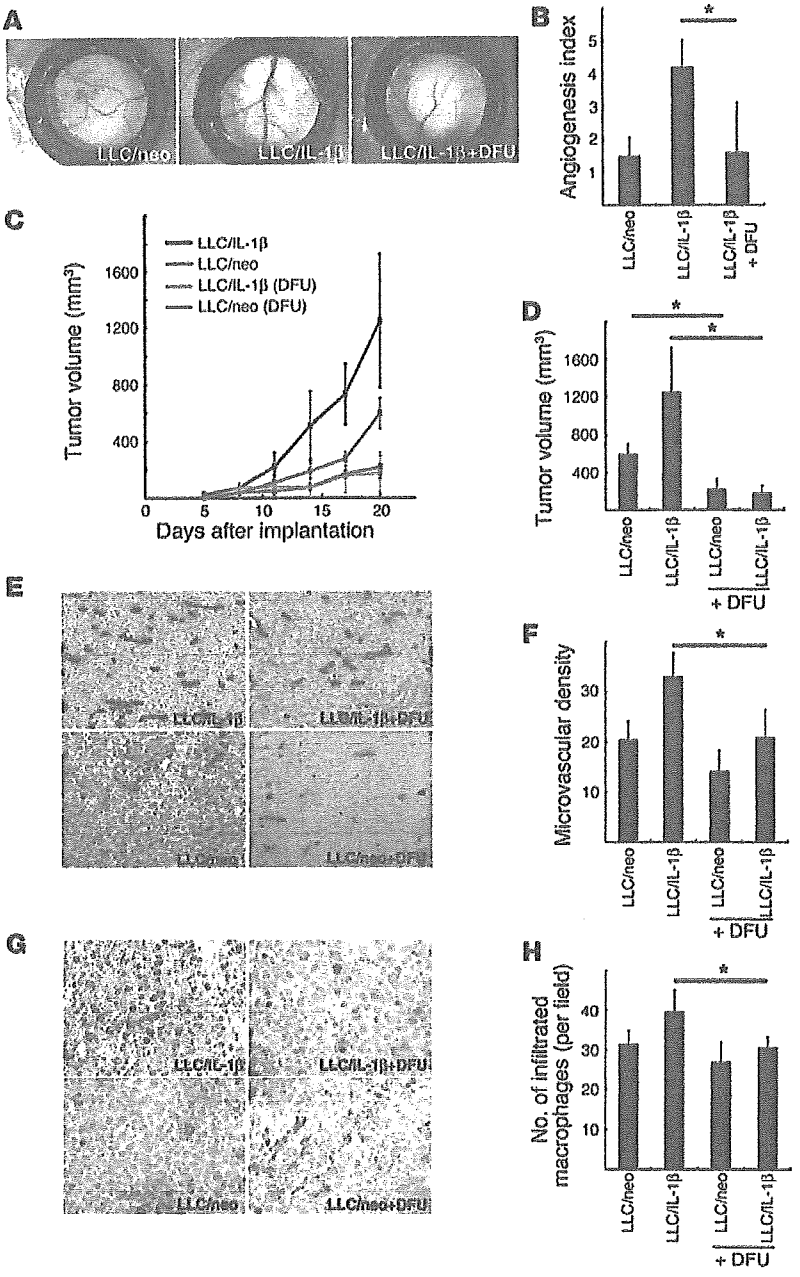

Figure 8
The effect of a COX-2 inhibitor on IL-1β–induced tumor angiogenesis. (**A**) Representative photographs of dorsal air sac assays in BALB/c mice with LLC/neo and LLC/IL-1β untreated or treated with DFU. (**B**) Quantitative analysis of the neovascularization induced by LLC/neo or LLC/IL-1β in the dorsal air sac assay in mice untreated or treated with DFU. Mean angiogenesis activities ± SD for groups of mice (n = 5). *P < 0.01 versus LLC/IL-1β. (**C**) Tumor volumes in wild-type mice implanted with 5 × 10^5 LLC/IL-1β or LLC/neo cells, untreated or treated with DFU. (**D**) LLC/IL-β and LLC/neo tumor growth was inhibited in DFU-treated mice compared with control mice (day 20). *P < 0.01 using unpaired Student's t test. (**E**) Representative photographs of CD31-stained tumor sections from LLC tumors grown in wild-type mice. Magnification, ×400. (**F**) CD31-positive microvascular densities from morphometric analysis of LLC tumors. Each value represents the mean number of vessels ± SD in 5 fields. *P < 0.01. (**G**) Infiltration of macrophages stained with mAb F4/80 in LLC/neo and LLC/IL-1β tumors in the mice indicated. Magnification, ×200. (**H**) Quantification of macrophages infiltrating LLC/IL-1β and LLC/neo tumors under the microscope. Magnification, ×400. Each value represents the mean number of macrophages ± SD in 5 fields. *P < 0.01 versus LLC/IL-1β wild-type mice using the Mann-Whitney U test.

mice, F4/80$^+$ macrophage infiltration into IL-1β–implanted corneas was observed after day 4. The number of infiltrating macrophages increased 2 days after IL-1β treatment and peaked on day 4. We previously demonstrated maximum levels of MIP-1α (a potent chemoattractant) and VEGF in mouse corneas 0.5–1 days after cauterization by silver nitrate. The infiltration of macrophages peaked on day 3, and neovascularization peaked on day 5 (45). These results suggest that the expression of potent attractants (such as MCP-1 and MIP-1α) 0.5–1 days after the presentation of inflammatory stimuli influences the subsequent appearance of macrophages. Determining the causative link between these processes in vivo will require further studies.

On day 2, dilated vascular loop structures were observed in MCP-1$^{-/-}$ and wild-type mice whereas vessel sprouts were not present on days 4 or 6 (Figure 3D). The appearance of dilated loop structures might not directly affect angiogenesis, and the underlying mechanism remains unclear. Cl_2MDP-LIPs reduced the appearance of IL-1β–induced vascular sprouts compared with controls on day 4 and decreased the corneal neovascularization on day 6. Macrophages might therefore be important for the sprouting and maintenance of IL-1β–induced neovascularization.

IL-1β reportedly induced MCP-1 expression in endothelial cells (32). We observed increased MCP-1 levels in the serum of LLC/IL-1β–grafted wild-type mice compared with LLC/neo-grafted wild-type mice (Figure 6). Only a slight increase in MCP-1 was observed in LLC/IL-1β–grafted MCP-1$^{-/-}$ mice. MCP-1 expression is reportedly associated with macrophage accumulation in various human cancers (46). Here we demonstrated that IL-1β– but not VEGF-induced corneal neovascularization was inhibited in MCP-1$^{-/-}$ mice. Moreover, LLC/IL-1β but not LLC/neo tumor growth was inhibited. Macrophage infiltration in IL-1β–implanted corneas and LLC/IL-1β tumor growth were impaired in MCP-1$^{-/-}$ mice compared with wild-type mice. Thus, the IL-1β–induced recruitment of angiogenic macrophages depended upon the upregulation of MCP-1 in vivo. MCP-1 appears to be pivotal in proinflammatory cytokine-induced angiogenesis and tumor growth, possibly through enhancing macrophage infiltration (Figure 10).

Lu et al. reported similar hematologic profiles in MCP-1$^{-/-}$ and wild-type mice (13). Low et al. demonstrated that MCP-1$^{-/-}$ leukocytes proliferated normally when stimulated in vitro (15). Freshly isolated monocytes from healthy donors expressed CCR2, but MCP-1 suppressed this during their differentiation into macrophages in vitro (47). The number of infiltrating macrophages in

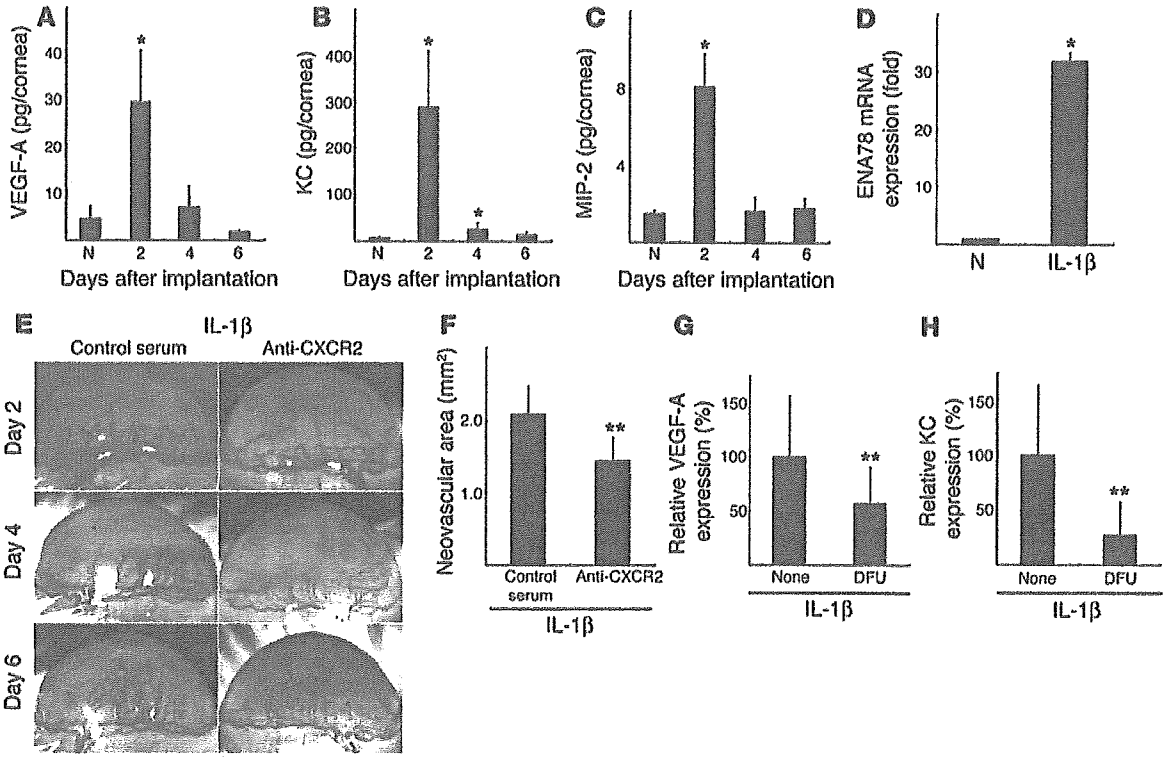

Figure 9

The effect of anti-CXCR2 Ab on IL-1β–induced angiogenesis. Kinetics of protein expression for (**A**) VEGF-A, (**B**) KC (mouse CXCL1), and (**C**) MIP-2 (mouse CXCL2/3) after IL-1β pellet implantation. Four corneal lysates were prepared and assayed by ELISA on the indicated days ($n = 3$). $^*P < 0.01$ versus untreated. (**D**) Expression of ENA-78 (CXCL5) mRNA levels in IL-1β–treated corneas. Six IL-1β–implanted corneas (IL-1β) or untreated corneas (N) were harvested, and real-time RT-PCR was performed to determine ENA-78 (CXCL5) mRNA levels on day 2. Expression was normalized to GAPDH mRNA levels. $^*P < 0.01$ versus untreated. (**E**) Corneal neovascularization on days 2, 4, and 6 in BALB/c mice with or without i.p. administration of anti-mouse CXCR2 Ab. (**F**) Quantitative analysis of neovascularization on day 6. IL-1β–induced corneal neovascularization in mice ($n = 6$) receiving anti-mouse CXCR2 Ab was inhibited compared with mice ($n = 6$) receiving control goat serum. $^{**}P < 0.05$ using Student's t test. (**G** and **H**) Comparison of levels of VEGF-A (**G**) and KC (**H**) in IL-1β–implanted corneas with or without DFU. On day 4, corneal lysates were prepared from 4 IL-1β–implanted corneas from DFU-treated and untreated mice and individually assayed by ELISA for VEGF-A or KC ($n = 3$). $^{**}P < 0.05$ using Student's t test.

MCP-1$^{-/-}$ mice was lower compared with wild-type mice after IL-1β treatment. MCP-1 deficiency might affect both macrophage recruitment and differentiation. Further studies will be required to establish the role of MCP-1 in macrophage differentiation.

Lyden et al. (48) reported the infiltration of Flt-1–positive monocytes in LLC-induced tumors. Anti-Flt-1 Ab inhibited their growth, suggesting that VEGF might promote monocyte/macrophage infiltration (48). VEGF induces the migration of VEGF-receptor 1–positive (VEGFR1-positive) and Flt-1–positive myelomonocytic cells (2, 49). Cursiefen et al. reported that VEGF functions in macrophage infiltration in injury-induced neovasculature in mouse corneas (19). Here, the VEGF-induced angiogenesis in mouse corneas was reduced by approximately 50% 6 days after Cl_2MDP-LIP treatment, and IL-1β–induced angiogenesis was blocked. VEGF-induced angiogenesis in mouse corneas might be partly due to the infiltration of macrophages: 2- to 3-fold increases occurred in monocyte/macrophage infiltration on days 4 and 6 after VEGF treatment, which might function in angiogenesis. VEGF- but not MCP-1–induced chemotaxis of human monocytes was inhibited by the VEGF receptor tyrosine kinase inhibitor SU5416 through Flt-1 (50). We recently confirmed that SU5416 partially blocked IL-1β–induced angiogenesis in mouse corneas (31).

COX-2 is pivotal in IL-1β–induced angiogenesis in vitro and in vivo (31). The enhanced production of prostanoids, such as PGE_2 and thromboxane A_2 (TXA_2), in response to IL-1β could promote angiogenesis, suggesting a model in which IL-1β–induced angiogenesis is mediated through both prostanoids and angiogenic factors (31). Pold et al. reported that COX-2 upregulated the expression of CXCL8 (IL-8) and CXCL5 (ENA-78) in non–small cell lung cancer cells in vitro and in vivo (38). The IL-1β–induced upregulation of IL-8 in lung cancer cells was blocked by anti-PGE_2 mAb (38). KC and VEGF-A were decreased in IL-1β–implanted corneas treated with DFU (Figure 9, G and H). This inflammatory cytokine-induced angiogenesis might be partially attributable to upregulation of VEGF-A and KC through the COX-2–activation pathway. CXC chemokines are known to induce angiogenesis (35). Addison et al. demonstrated the angiogenic activity of ELR$^+$ CXC chemokines through CXCR2 (36). Saijo et al. showed that treatment with anti-CXCR2 Ab inhibited IL-1β–induced tumor growth in mice (6). Keane et al. demonstrated that CXC chemokines modulated tumor growth through angiogenesis by indirect effects on tumor cells or leukocytes in CXCR2$^{-/-}$ mice (51). Our corneal model revealed that IL-1β increased the expression of both CXC chemokines and VEGF-A (Figure 9). Furthermore, IL-1β–induced

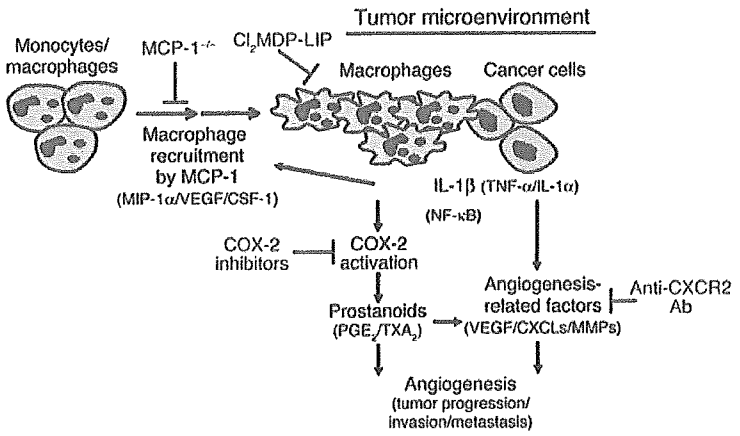

Figure 10

Model of the involvement of macrophages in IL-1β–induced angiogenesis in the tumor microenvironment. Monocytes/macrophages are expected to be recruited to the tumor environment in response to IL-1β and possibly other chemokines that attract macrophages. COX-2 activation is then induced, and the macrophages promote angiogenesis and tumor progression. Signaling molecules downstream of COX-2, PGE_2, and TXA_2 enhance the production of various angiogenesis-related factors (37, 38). IL-1β, IL-1α, and TNF-α enhance the expression of angiogenesis-related factors in cancer and vascular endothelial cells resulting from autocrine and/or paracrine controls in angiogenesis (5, 30, 55, 56). Monocytes/macrophages are recruited to the tumor environment in response to MCP-1 (and possibly MIP-1α, VEGF/PlGF, and CSF-1) accompanied by COX-2 activation in infiltrating macrophages by IL-1β (and possibly IL-1α and/or TNF-α). As a result, angiogenesis is enhanced by prostanoids (such as PGE_2 and TXA_2) as well as other angiogenic factors (such as VEGF, CXC chemokines, and MMPs). Clodronate blocks inflammatory angiogenesis induced by IL-1β.

corneal angiogenesis was partially inhibited by anti-CXCR2 Ab. CXC chemokines, prostanoids, and VEGF-A could therefore all be involved in IL-1β–induced angiogenesis.

Many COX-2–positive cells infiltrate the IL-1β–induced neovasculature in mouse corneas (31). Here, macrophage infiltration was enhanced in response to IL-1β compared with VEGF. Infiltrating macrophages around the IL-1β–induced neovasculature expressed COX-2, whereas those surrounding preexisting vessels did not. The number of infiltrating macrophages was higher in LLC/IL-1β tumors than in LLC/neo tumors in vivo. Our study revealed several features of the role of COX-2 production in tumor angiogenesis. LLC/IL-1β–induced angiogenesis in vivo was blocked by a COX-2 inhibitor. LLC/IL-1β tumor growth and induced microvascularization were specifically blocked by the COX-2 inhibitor. Macrophage infiltration in LLC/IL-1β–induced tumors was significantly blocked by a COX-2 inhibitor compared with wild-type mice. These findings suggest that IL-1β–driven tumor angiogenesis and tumor growth depend on macrophage infiltration as well as COX-2–positive tumor-associated macrophages and possibly cancer cells with high COX-2 expression (Figure 10). However, inhibition of COX-2 activity only weakly influenced macrophage infiltration in response to IL-1β in cancer (Figure 8). The decrease in angiogenesis and tumor growth by LLC/IL-1β induced by a COX-2 inhibitor could be specifically associated with COX-2 activity in macrophages and other cell types rather than the number of infiltrating macrophages at or near the site of tumor growth. The infiltration of tumor-associated or tumor-educated macrophages is often associated with disease progression or poor prognosis for cancer patients. These activated macrophages appear to be important in tumor angiogenesis (16, 30, 46, 52). An experimental model system with LLC/IL-1β showed IL-1β to be essential for tumor angiogenesis, invasion, and metastasis as well as immunosuppression (6–8). COX-2–positive macrophages activated in the inflammatory microenvironment might be critical for acquiring a malignant phenotype in cancer. COX-2–positive macrophages could thus be target cells for future anticancer therapeutic strategies

In conclusion, IL-1β induced angiogenesis with a concomitant infiltration of macrophages, most of which were COX-2 positive. Macrophage depletion through treatment with a targeted drug or using MCP-$1^{-/-}$ mice abrogated IL-1β–induced angiogenesis. This complex process involves multiple redundant and interconnected pathways. It is therefore remarkable that macrophage depletion alone almost abolished IL-1β–induced corneal neovascularization and tumor growth.

Methods

Animals. All animal experiments were approved by the Committee on the Ethics of Animal Experiments, Kyushu University Graduate School of Medical Sciences, Japan. Male BALB/c and C57BL/6 mice (6–10 weeks old) were purchased from Seac Yoshitomi Ltd. MCP-$1^{-/-}$ mice were kindly provided by B.J. Rollins (Harvard Medical School, Boston, Massachusetts, USA).

Corneal micropocket assay in mice. The mouse corneal micropocket assay and quantification of neovascularization were performed as described previously (31, 53).

Immunohistochemistry. Mice were sacrificed under deep anesthesia with pentobarbital sodium (60 mg/kg i.p.). The eyes were removed, snap-frozen in OCT compound (Sakura Finetechnical Co.), and 5-μm sections were cut, air dried, and fixed in cold acetone for 10 minutes. The sections were blocked with 3% BSA and labeled at room temperature with rat anti-mouse Gr-1 (550291) or rat anti-mouse CD31 (550274; BD Biosciences) for 1 hour, followed by biotinylated goat anti-rat Ig (559286; BD Biosciences) for 20 minutes. Frozen sections were labeled with biotinylated anti-F4/80 for 1 hour. The sections were treated with horseradish peroxidase–conjugated streptavidin (1:1000; Jackson ImmunoResearch Laboratories Inc.) and 3,3′-diaminobenzidine substrate (BioGenex Laboratories). Frozen sections were also stained with rat anti-mouse F4/80 (MCA497R; Serotec) or anti-Gr-1 and rabbit anti-mouse COX-2 Ab (160126; Cayman Chemical Co.).

Isolation of cornea-infiltrating cells and flow cytometry. Inflammatory cells were isolated from the corneas as described previously (54). For 3-color flow cytometry, corneal infiltrating cells were stained with the following: PE-CD11b mAb (RM2804; CALTAG Laboratories) to label macrophages and neutrophils or PE-anti-CD11c mAb (557401; BD Biosciences) to label dendritic cells; either FITC-anti-Gr-1 (551460; BD Biosciences) to label neutrophils or FITC-anti-F4/80 mAb (RM2901; CALTAG Laboratories) to label macrophages; and propidium iodide (BD Biosciences).

ELISAs. Groups of 4 corneas were removed and dissected with scissors. The supernatants were assayed in ELISA kits for mouse MCP-1 (KMC1010-SB; BioSource International), mouse KC (MKC00B; R&D Systems), mouse MIP-2 (MM200; R&D Systems), and mouse VEGF-A (MMV00; R&D Systems).

Liposomes. Cl_2MDP-LIPs were prepared as previously described (23). Animals received 200 μl Cl_2MDP-LIPs or PBS-LIPs i.v. in the retro-orbital plexus with a 26-gauge needle on days –2, 0, 2, and 4. They also received 10

μl Cl_2MDP-LIPs in 1 eye and 10 μl PBS-LIPs in the other, injected into the s.c. space. All injections were masked.

Mouse dorsal air sac assay. A dorsal air sac assay was performed according to the method published previously (50). Five mice in each group were sacrificed and skinned on day 6. We counted the number of meandering blood vessels within the chamber in the area of the air sac fascia and graded the angiogenic response from 0 to 5, respectively.

Quantitative real-time RT-PCR. Total RNA was extracted from 6 corneas by ISOGEN (317-02503; Nippon Gene Co.), and quantitative RT-PCR was performed in duplicate using mouse ENA-78–specific TaqMan primers and probes and the ABI Prism 7300 sequence detector (Applied Biosystems).

Statistics. All results are expressed as mean ± SEM. The statistical significance of differences between groups was analyzed by 2-tailed Student's *t* test or Mann-Whitney *U* test. Differences were considered significant at $P < 0.05$, and each experiment was performed at least twice.

Acknowledgments

We thank R. Kono, T. Oshima, M. Imamura, and M. Takahara (Kyushu University) for technical support and N. Shinbaru (Kyushu University) for editorial help. This work was supported by the Third-Term Comprehensive Ten-Year Strategy for Cancer Control from the Ministry of Health, Welfare, and Labor of Japan.

Received for publication September 4, 2004, and accepted in revised form August 23, 2005.

Address correspondence to: Mayumi Ono, Department of Medical Biochemistry, Graduate School of Medical Science, Kyushu University, 3-1-1 Maidashi, Higashi-ku, Fukuoka 812-8582, Japan. Phone: 81-92-642-6098; Fax: 81-92-642-6203; E-mail: mayumi@biochem1.med.kyushu-u.ac.jp.

1. Carmeliet, P. 2003. Angiogenesis in health and disease. *Nat. Med.* **9**:653–660.
2. Rafii, S., and Lyden, D. 2003. Therapeutic stem and progenitor cell transplantation for organ vascularization and regeneration. *Nat. Med.* **9**:702–712.
3. Dinarello, C.A. 1996. Biologic basis for interleukin-1 in disease. *Blood.* **87**:2095–2147.
4. Mantovani, A., Bussolino, F., and Dejana, E. 1992. Cytokine regulation of endothelial cell function. *FASEB J.* **6**:2591–2599.
5. Torisu, H., et al. 2000. Macrophage infiltration correlates with tumor stage and angiogenesis in human malignant melanoma: possible involvement of TNFalpha and IL-1alpha. *Int. J. Cancer.* **85**:182–188.
6. Saijo, Y., et al. 2002. Proinflammatory cytokine IL-1 beta promotes tumor growth of Lewis lung carcinoma by induction of angiogenic factors: in vivo analysis of tumor-stromal interaction. *J. Immunol.* **169**:469–475.
7. Yano, S., et al. 2003. Multifunctional interleukin-1beta promotes metastasis of human lung cancer cells in SCID mice via enhanced expression of adhesion-, invasion- and angiogenesis-related molecules. *Cancer Sci.* **94**:244–252.
8. Voronov, E., et al. 2003. IL-1 is required for tumor invasiveness and angiogenesis. *Proc. Natl. Acad. Sci. U. S. A.* **100**:2645–2650.
9. Bar, D., Apte, R.N., Voronov, E., Dinarello, C.A., and Cohen, S.A. 2004. Continuous delivery system of IL-1 receptor antagonist reduces angiogenesis and inhibits tumor development. *FASEB J.* **18**:161–163.
10. Song, X., et al. 2003. Differential effects of IL-1 alpha and IL-1 beta on tumorigenicity patterns and invasiveness. *J. Immunol.* **171**:6448–6456.
11. Shaw, J.P., Chuang, N., Yee, H., and Shamamian, P. 2003. Polymorphonuclear neutrophils promote rFGF-2-induced angiogenesis in vivo. *J. Surg. Res.* **109**:37–42.
12. Fuentes, M.E., et al. 1995. Controlled recruitment of monocytes and macrophages to specific organs through transgenic expression of monocyte chemoattractant protein-1. *J. Immunol.* **155**:5769–5776.
13. Lu, B., et al. 1998. Abnormalities in monocyte recruitment and cytokine expression in monocyte chemoattractant protein 1-deficient mice. *J. Exp. Med.* **187**:601–608.
14. Huang, D.R., Wang, J., Kivisakk, P., Rollins, B.J., and Ransohoff, R.M. 2001. Absence of monocyte chemoattractant protein 1 in mice leads to decreased local macrophage recruitment and antigen-specific T helper cell type 1 immune response in experimental autoimmune encephalomyelitis. *J. Exp. Med.* **193**:713–726.
15. Low, Q.E., et al. 2001. Wound healing in MIP-1 alpha(-/-) and MCP-1(-/-) mice. *Am. J. Pathol.* **159**:457–463.
16. Coussens, L.M., and Werb, Z. 2002. Inflammation and cancer. *Nature.* **420**:860–867.
17. Tsutsumi, C., et al. 2003. The critical role of ocular-infiltrating macrophages in the development of choroidal neovascularization. *J. Leukoc. Biol.* **74**:25–32.
18. Moulton, K.S., et al. 2003. Inhibition of plaque neovascularization reduces macrophage accumulation and progression of advanced atherosclerosis. *Proc. Natl. Acad. Sci. U. S. A.* **100**:4736–4741.
19. Cursiefen, C., et al. 2004. VEGF-A stimulates lymphangiogenesis and hemangiogenesis in inflammatory neovascularization via macrophage recruitment. *J. Clin. Invest.* **113**:1040–1050. doi:10.1172/JCI200420465.
20. Leek, R.D., et al. 1996. Association of macrophage infiltration with angiogenesis and prognosis in invasive breast carcinoma. *Cancer Res.* **56**:4625–4629.
21. Toi, M., et al. 1999. Significance of thymidine phosphorylase as a marker of protumor monocytes in breast cancer. *Clin. Cancer Res.* **5**:1131–1137.
22. Nishie, A., et al. 1999. Macrophage infiltration and heme oxygenase-1 expression correlate with angiogenesis in human gliomas. *Clin. Cancer Res.* **5**:1107–1113.
23. Lissbrant, I.F., et al. 2000. Tumor associated macrophages in human prostate cancer: relation to clinicopathological variables and survival. *Int. J. Oncol.* **17**:445–451
24. Salvesen, H.B., and Akslen, L.A. 1999. Significance of tumour-associated macrophages, vascular endothelial growth factor and thrombospondin-1 expression for tumour angiogenesis and prognosis in endometrial carcinomas. *Int. J. Cancer.* **84**:538–543.
25. Fujimoto, J., Sakaguchi, H., Aoki, I., and Tamaya, T. 2000. Clinical implications of expression of interleukin 8 related to angiogenesis in uterine cervical cancers. *Cancer Res.* **60**:2632–2635.
26. Koukourakis, M.I., et al. 1998. Different patterns of stromal and cancer cell thymidine phosphorylase reactivity in non-small-cell lung cancer: impact on tumour neoangiogenesis and survival. *Br. J. Cancer.* **77**:1696–1703.
27. Hanada, T., et al. 2000. Prognostic value of tumor-associated macrophage count in human bladder cancer. *Int. J. Urol.* **7**:263–269.
28. Torisu-Itakura, H., Furue, M., Kuwano, M., and Ono, M. 2000. Co-expression of thymidine phosphorylase and heme oxygenase-1 in macrophages in human malignant vertical growth melanomas. *Jpn. J. Cancer Res.* **91**:906–910.
29. SunderKotter, C., Steinbrink, K., Goebeler, M., Bhardwaj, R., and Sorg, C. 1994. Macrophages and angiogenesis. *J. Leukoc. Biol.* **55**:410–422.
30. Ono, M., Torisu, H., Fukushi, J., Nishie, A., and Kuwano, M. 1999. Biological implications of macrophage infiltration in human tumor angiogenesis. *Cancer Chemother. Pharmacol.* **43**(Suppl.):S69–S71.
31. Kuwano, T., et al. 2004. Cyclooxygenase 2 is a key enzyme for inflammatory cytokine induced angiogenesis. *FASEB J.* **18**:300–310.
32. Sica, A., et al. 1990. Monocyte chemotactic and activating factor gene expression induced in endothelial cells by IL-1 and tumor necrosis factor. *J. Immunol.* **144**:3034–3038.
33. Van Rooijen, N., and Sanders, A. 1994. Liposome mediated depletion of macrophages: mechanism of action, preparation of liposomes and applications *J. Immunol. Methods.* **174**:83–93.
34. Sakurai, E., Anand, A., Ambati, B.K., van Rooijen, N., and Ambati, J. 2003. Macrophage depletion inhibits experimental choroidal neovascularization. *Invest. Ophthalmol. Vis. Sci.* **44**:3578–3585.
35. Strieter, R.M., et al. 1995. The functional role of the 'ELR' motif in CXC chemokine-mediated angiogenesis. *J. Biol. Chem.* **270**:27348–27357.
36. Addison, C.L., et al. 2000. The CXC chemokine receptor 2, CXCR2, is the putative receptor for ELR$^+$ CXC chemokine-induced angiogenic activity. *J. Immunol.* **165**:5269–5277.
37. Williams, C.S., Tsujii, M., Reese, J., Dey, S.K., and DuBois, R.N. 2000. Host cyclooxygenase-2 modulates carcinoma growth. *J. Clin. Invest.* **105**:1589–1594.
38. Pold, M., et al. 2004. Cyclooxygenase-2-dependent expression of angiogenic CXC chemokines ENA-78/CXC ligand (CXCL) 5 and interleukin-8/CXCL8 in human non-small cell lung cancer. *Cancer Res.* **64**:1853–1860.
39. Li, B.Y., et al. 1992. Human ovarian epithelial cancer cell cultures in vitro express both interleukin 1 alpha and beta genes. *Cancer Res.* **52**:2248–2252.
40. Yoshida, N., et al. 2002. Interleukin-6, tumour necrosis factor alpha and interleukin-1beta in patients with renal cell carcinoma. *Br. J. Cancer.* **86**:1396–1400.
41. Kabir, S., and Daar, G.A. 1995. Serum levels of interleukin-1, interleukin-6 and tumour necrosis factor-alpha in patients with gastric carcinoma. *Cancer Lett.* **95**:207–212.
42. Conejo-Garcia, J.R., et al. 2004. Tumor-infiltrating dendritic cell precursors recruited by a β-defensin contribute to vasculogenesis under the influence of Vegf-A. *Nat. Med.* **10**:950–958.
43. Zhang, Y., et al. 2002. APCs in the liver and spleen recruit activated allogeneic CD8$^+$ T cells to elicit hepatic graft-versus-host disease. *J. Immunol.* **169**:7111–7118.
44. Cheng, H., et al. 2000. Role of macrophages in restricting herpes simplex virus type 1 growth after ocular infection. *Invest. Ophthalmol. Vis. Sci.* **41**:1402–1409.
45. Ogawa, S., et al. 1999. Induction of macrophage inflammatory protein-1alpha and vascular endothelial growth factor during inflammatory

neovascularization in the mouse cornea. *Angiogenesis.* **3**:327–334.
46. Ueno, T., et al. 2000. Significance of macrophage chemoattractant protein-1 in macrophage recruitment, angiogenesis, and survival in human breast cancer. *Clin. Cancer Res.* **6**:3282–3289.
47. Fantuzzi, L., et al. 1999. Loss of CCR2 expression and functional response to monocyte chemotactic protein (MCP-1) during the differentiation of human monocytes: role of secreted MCP-1 in the regulation of the chemotactic response. *Blood.* **94**:875–883.
48. Lyden, D., et al. 2001. Impaired recruitment of bone-marrow-derived endothelial and hematopoietic precursor cells blocks tumor angiogenesis and growth. *Nat. Med.* **7**:1194–1201.
49. Sawano, A., et al. 2001. Flt-1, vascular endothelial growth factor receptor 1, is a novel cell surface marker for the lineage of monocyte-macrophages in humans. *Blood.* **97**:785–791.
50. Itokawa, T., et al. 2002. Antiangiogenic effect by SU5416 is partly attributable to inhibition of Flt-1 receptor signaling. *Mol. Cancer Ther.* **1**:295–302.
51. Keane, M.P., Belperio, J.A., Xue, Y.Y., Burdick, M.D., and Strieter, R.M. 2004. Depletion of CXCR2 inhibits tumor growth and angiogenesis in a murine model of lung cancer. *J. Immunol.* **172**:2853–2860.
52. Pollard, J.W. 2004. Tumour-educated macrophages promote tumour progression and metastasis. *Nat. Rev. Cancer.* **4**:71–78.
53. Nakao, S., Kuwano, T., Ishibashi, T., Kuwano, M., and Ono, M. 2003. Synergistic effect of TNF-alpha in soluble VCAM-1-induced angiogenesis through alpha 4 integrins. *J. Immunol.* **170**:5704–5711.
54. Sonoda, K., et al. 1998. Inhibition of corneal inflammation by the topical use of Ras farnesyltransferase inhibitors: selective inhibition of macrophage localization. *Invest. Ophthalmol. Vis. Sci.* **39**:2245–2251.
55. Ryuto, M., et al. 1996. Induction of vascular endothelial growth factor by tumor necrosis factor alpha in human glioma cells. Possible roles of SP-1. *J. Biol. Chem.* **271**:28220–28228.
56. Yoshida, S., et al. 1997. Involvement of interleukin-8, vascular endothelial growth factor, and basic fibroblast growth factor in tumor necrosis factor alpha-dependent angiogenesis. *Mol. Cell. Biol.* **17**:4015–4023.

Antineoplaston induces G_1 arrest by PKCα and MAPK pathway in SKBR-3 breast cancer cells

TERUHIKO FUJII[1,2], ANNA M. NAKAMURA[2], GORO YOKOYAMA[1,2], MIKI YAMAGUCHI[1,2], KOSUKE TAYAMA[1], KEISUKE MIWA[1], UHI TOH[1], DAISUKE KAWAMURA[1], KAZUO SHIROUZU[1], HIDEAKI YAMANA[2,3], MICHIHIKO KUWANO[2] and HIDEAKI TSUDA[4]

[1]Department of Surgery, [2]Research Center for Innovative Cancer Therapy of the 21st Century COE Program for Medical Science, [3]Multidisciplinary Treatment Center, Kurume University School of Medicine, 67 Asahimachi, Kurume, Fukuoka 830-0011; [4]Department of Anesthesiology, Kurume Daiichi Social Insurance Hospital, 21 Kushiharamachi, Kurume, Fukuoka 830-0013, Japan

Received February 15, 2005; Accepted April 15, 2005

Abstract. Antineoplastons such as A10 include naturally occurring peptides and amino acid derivatives that control the neoplastic growth of cells. The mechanism underlying this antitumor effect was investigated using the breast cancer cell line, SKRB-3. Cells treated with A10 were monitored for any changes in cell cycle, expression of protein kinase C (PKC), or intracellular signal transduction, particularly phosphorylation of mitogen-activated protein kinase (MAPK). The A10 markedly inhibited SKBR-3 proliferation due to arrest in the G_1 phase. A10 down-regulated the expression of PKCα protein, resulting in inhibition of extracellular signal-regulated kinase (ERK) MAPK phosphorylation. This increased the expression of p16 and p21 protein, with resultant inhibition of Rb phosphorylation, leading to G_1 arrest. This study has defined a pathway in which A10 arrested SKBR-3 cells in the G_1 phase via PKCα and MAPK. Our findings indicate that the antineoplaston A10 antitumor effect could be utilized as an effective therapy for breast cancer patients.

Introduction

Antineoplastons are naturally occurring peptides, amino acid derivatives and organic acids, found in blood, tissue and urine. Their inhibitory effect on neoplastic cell growth was first described in 1976 (1). The first synthetic antineoplaston was produced from extracted antineoplaston A2 and designated A10. Its chemical composition is 3-phenylacetylamino-2, 6-piperidinedione and it is hydrolized in pancreatic juice to phenylacetylglutamine and phenylacetylisoglutamine. Clinical studies have described the effectiveness of antineoplastons on many different tumors (2-6). Moreover, Badria *et al* reported that A10 significantly inhibited neutrophil apoptosis in breast cancer patients (7). The mechanism underlying the antitumor effect is considered to involve regulation of p53 and p21 gene expression through demethylation of their promoter sequences and acetylation of histones (2). However, both the mechanism and effect on breast cancer cells have been poorly studied to date. The present study examined the effect of antineoplaston A10 on protein kinase C (PKC) and mitogen-activated protein kinase (MAPK) which are directly involved in cell growth during breast cancer.

PKCs are phospholipid dependent serine/threonine kinase that are involved in regulating basic cell functions, such as proliferation and differentiation (8). At least 11 isozymes of PKC have been described (α, ßI, ßII, γ, δ, ε, η, θ, ζ and λ/ι) (9-12), and are divided into three subgroups. PCKα, ßI, ßII and γ are considered to be the classical PKC (cPKC) isozymes, which are activated by calcium and diacylglycerol (DAG)/phorbol esters. PKCδ, ε, η and θ are classified as novel PKC (nPKC) isozymes; they are also activated by DAG and phorbol esters, but their activation is not dependent on calcium. PKCζ and λ/ι are atypical PKC (aPKC) isozymes which are not dependent on calcium, DAG, or phorbol esters. When a certain stimulus is applied to the cell membrane, phospholipase C, an effector, is activated via G protein. As a result, phosphatidylinositol-4,5-bisphosphate (PIP_2), which is a trace component of the cell membrane, is broken down to DAG, which in turn activates cPKC and nPKC, leading to phosphorylation of substrates downstream (12-14). Particularly in breast cancer cells, PKCα is the primary target of PMA, which acts as a transient negative regulator of cell spreading and motility. This was shown specifically in MDA-MB-231 cells (15). The endogenous PKCα in MCF-7 cells plays a critical role in regulating cell-cycle control and apoptosis, in part through up-regulating the expression of p21CIP1 and

Correspondence to: Dr Teruhiko Fujii, Department of Surgery, Kurume University School of Medicine, 67 Asahimachi, Kurume, Fukuoka, 830-0011, Japan
E-mail: tfujii@med.kurume-u.ac.jp

Key words: SKBR-3 breast cancer cells, antineoplaston, G_1 arrest, PKC, ERK MAPK

bcl-2 (16). Moreover, the interaction between PKCη and cyclin E is carefully regulated, and it correlates with the inactive form of the cyclin E/Cdk2 complex (17). An atypical PKCζ blocks the phosphorylation of Akt in breast cancer cells (18). These data strongly suggest that PKC is involved in the proliferation, differentiation and death of breast cancer cells.

The mitogen-activated protein kinase (MAPK) family consists of extracellular signal-regulated kinase (ERK) MAPK, c-jun NH_2-terminal kinase (JNK) and p38. The protein kinase cascade is activated in response to various external stimuli and transfers extracellular signals to the nuclei. Various cellular responses, such as proliferation, differentiation and cell death, are controlled by the regulation of gene expression by MAPK. ERK MAPK is considered to function in cell proliferation and differentiation. It is a focus of research relating to carcinogenesis, particularly because of activation by downstream signaling cascades of growth factors (19,20). It has also been shown in breast cancer cells, that HER2 and PKCδ are involved in the activation of ERK MAPK induced by estrogen (21). Furthermore, angiotensin II induced, in a dosage-dependent manner, proliferation of breast cancer cells and acceleration of phosphorylation of ERK MAPK, secondary to translocation of PKCα, ß and δ. Therefore, it is assumed that there is a close relationship between PKC and MAPK. However, the potential role of PKC or MAPK as mediators of the antineoplaston effects in breast cancer cells have not yet been investigated in detail. If this relationship could be clarified in breast cancer cells, antineoplaston treatment could be an effective therapy for breast cancer patients.

The present study examined the effects of antineoplaston A10 on PKC and ERK MAPK signaling, as well as in the regulation of the cell cycle in the SKBR-3 human breast cancer cell line. Interestingly, we found that A10 caused G_1 arrest in SKBR-3 cells, and that PKCα and ERK MAPK were closely involved in the inhibition of cell proliferation.

Materials and methods

Materials. Antineoplaston A10 was provided by Dr S.R. Burzynski (Burzynski Research Institute, Inc.). PD98059 and Gö6976 were obtained from Alexis Corporation (San Diego, CA).

Cell culture and cell proliferation studies. The SKBR-3 breast cancer cell line, was obtained from the American Type Culture Collection (ATCC) (Manassas, VA), and was cultured in Dulbecco's modified Eagle's medium (DMEM) supplemented with 10% fetal bovine serum (FBS) at 37°C in an atmosphere of 5% CO_2.

Treatment of antineoplaston A10. To assess the effect of A10 on cell proliferation, concentrations of 1, 3 or 10 mg/ml were added to SKBR-3 cells in 6-well plates and incubated for 24-72 h. Cells were then suspended by treatment with 0.05% trypsin and counted using a hemocytometer.

Flow cytometry. Cells were fixed with 70% ethanol, stained with propidium iodide (1 mg/ml), and examined for changes in the cell cycle distribution using flow cytometry (FACScan, Becton-Dickinson, CA).

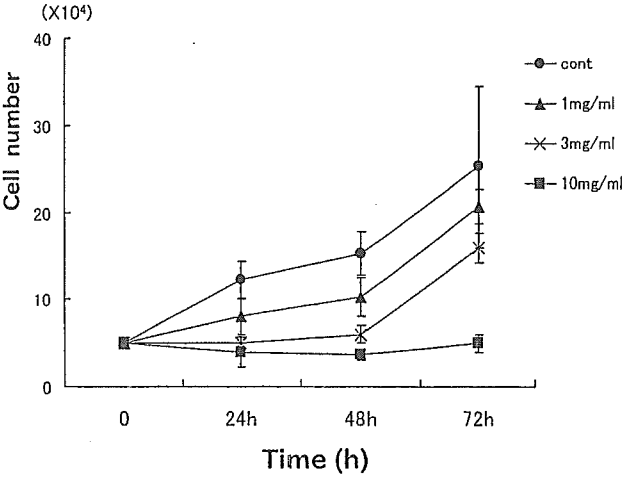

Figure 1. Effect of A10 on SKBR-3 cell growth. Different concentrations of A10 (1, 3 or 10 mg/ml) were added to SKBR-3 cells in 6-well plates for different incubation periods. The cell number was determined by hemocytometer counting. Data are expressed as the mean ± SE of three independent experiments.

Western blot analysis. Lysis buffer (50 mM Tris-HCl, pH 7.4, 1% NP-40, 0.25% Na-deoxycholate, 150 mM NaCl, 1 mM Na_3VO_4, 1 mM PMSF, 1 mM NaF, 1 μg/ml pepstatin) was added to SKBR-3 cells, and SDS-polyacrylamide gel slab electrophoresis was performed, followed by blotting onto a nitrocellulose membrane. Membranes were blocked for 1 h using tris-buffered saline (TBS) containing 5% milk and 0.1% Tween-20 and then incubated for 24 h with one of the following primary antibodies; anti-PKCα, δ, ε, ι, θ and ζ (1:1,000, Transduction Laboratories, Lexington, KY), anti-ERK MAPK (1:1,000, phosphospecific antibody and total antibody, New England Biolabs, Beverly, MA), anti-p16 (1:1,000, Santa Cruz Biotechnology, Santa Cruz, CA), anti-p21 (1:1,000, Santa Cruz Biotechnology), anti-p27 (1:1,000, Santa Cruz Biotechnology), anti-cyclin D1 (1:1,000, PharMingen, San Diego, CA), anti-cyclin E (1:1,000, PharMingen), anti-phosphospecific-retinoblastoma (Rb) (Ser807/811) (1:1,000, Cell Signaling Technology, Beverly, MA) and anti-ß-actin (1:1,000, Sigma, Saint Louis, MO). After washing three times with TBS containing 0.1% Tween-20, the membrane was incubated for 60 min with the secondary antibody (1:2,000, anti-mouse or anti-rabbit horseradish peroxidase, Bio-Rad, CA). Bands were detected using the enhanced chemiluminescence (ECL) Western blot detection system (Amersham Biosciences, Buckinghamshire, UK).

Statistical analysis. Statistical analysis was performed using the Student's t-test. A level of $p<0.05$ was considered statistically significant.

Results

A10 inhibits proliferation of SKBR-3 breast cancer cells. A10 caused the dose-dependent inhibition of SKBR-3 cells (Fig. 1). When compared to the control, cells incubated for 72 h with 1, 3 or 10 mg/ml A10 underwent 36 and 80% cell growth inhibition, respectively.

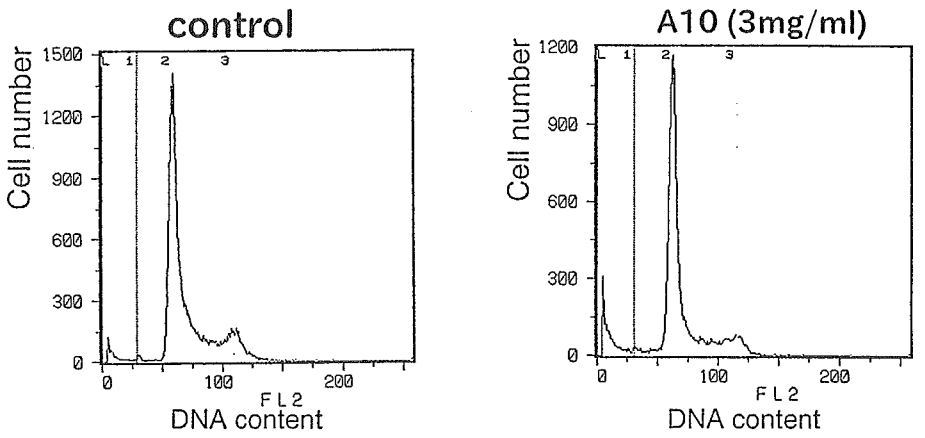

Phase	Control	A10 (3mg/ml)
G_0/G_1	44%	59%
S	48%	37%
G_2/M	8%	5%

Figure 2. A10-induced changes in the cell cycle. SKBR-3 cells were treated with 3 mg/ml A10 for 24 h, and then fixed with 70% ethanol, stained with propidium iodide (1 mg/ml), and examined for changes in the cell cycle distribution using flow cytometry. A representative experiment is shown. Similar results were obtained in two additional experiments.

Effects of A10 on cell cycle distribution. The cell growth curves and the flow cytometry results suggested that A10 inhibited the growth of SKBR-3 cells, and increased the proportion of cells in the G_0/G_1 phase, that is, they caused G_1 arrest. Analysis of the cell cycle showed that in the group without A10, 44% of the cells were in the G_0/G_1 phase, and 8% at the G_2/M phase. However, in the 3 mg/ml A10 group after 24 h, 59% of the cells were in the G_0/G_1 phase and 5% at the G_2/M phase, indicating that the percentage of G_0/G_1-phase cells had increased markedly (Fig. 2).

Effect of A10 on p16, p21, p27, cyclins and Rb. It has been suggested that SKBR-3 cells undergo G_1 arrest after A10 treatment, therefore we examined the expression of cell cycle regulators that are essential for G_0/G_1 progression. We focused on changes in p16, p21, p27, cyclin D1, cyclin E protein expression and phosphorylation of Rb protein. As a result, expression of p16 and p21 protein was increased at 12 h after the administration of A10 (Fig. 3), while there was no change in the expression of cyclin D1, cyclin E and p27 protein (data not shown). Furthermore, the phosphorylation of Rb at Ser807/811 was inhibited 24 h after A10 was administered (Fig. 3).

A10-induced changes in PKC expression and effect of the classical PKC inhibitor Gö6976. Since PKC is strongly related to cell growth we next investigated how A10 affects this enzyme. The expression of PKCα decreased at 30 min after 3 mg/ml A10 was added, but expression of other PKC proteins was unchanged (Fig. 4A). These results suggest that PKCα is

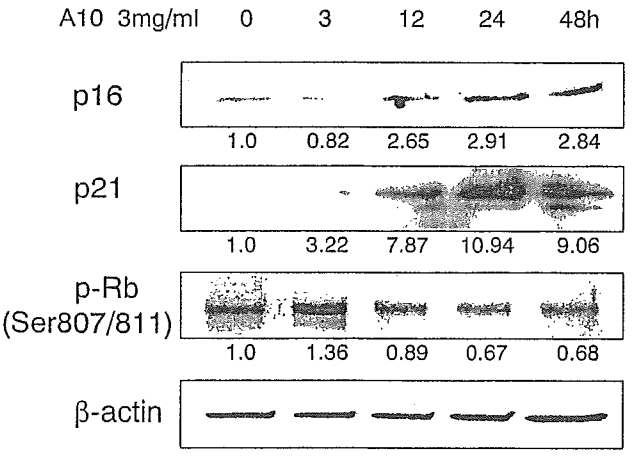

Figure 3. Effect of A10 on p16, p21 protein expression and Rb phosphorylation. SKBR-3 cells were treated with 3 mg/ml A10. Between 0 and 48 h, the expression of p16, p21 protein and Rb phosphorylation was examined by Western blotting. Similar results were observed in two additional experiments. Values indicate the density of the band.

involved in the control of SKBR-3 cell proliferation by A10. The potential role of PKCα isozymes in the A10-mediated control of SKBR-3 cell proliferation was evaluated using a classical PKC inhibitor, Gö6976. As SKBR-3 cells do not express PKCß or PKCγ (23), Gö6976 acted on them as a specific PKCα inhibitor. SKBR-3 cells were treated with vehicle (control), Gö6976 (3 μM) alone, or with a combination of A10 (3 mg/ml) and Gö6976 (3 μM). After 24 h, the cells

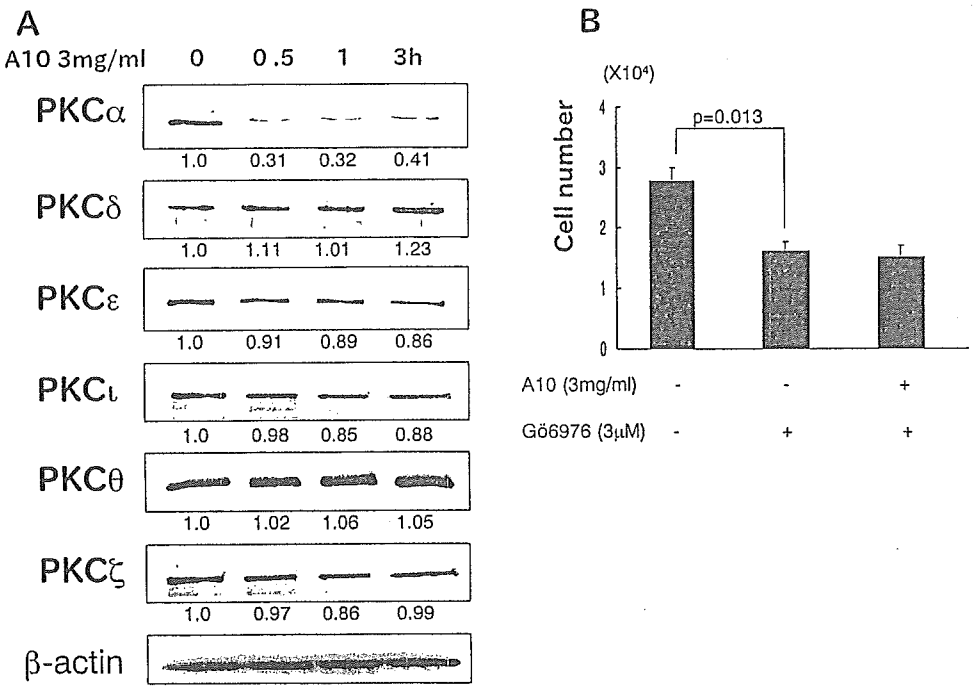

Figure 4. A10-induced changes in PKC isozymes and effect of Gö6976. (A) SKBR-3 cells were treated with A10 (3 mg/ml) for different periods, as detailed in the figure. Expression of PKC isozymes was determined by Western blotting using specific anti-PKC antibodies. Similar results were observed in two additional experiments. Values indicate the density of the band. (B) SKBR-3 cells were treated with vehicle (control), Gö6976 (3 μM) alone or with a combination of A10 (3 mg/ml) and Gö6976 (3 μM). After 24 h, the cells were suspended by treatment with 0.05 % trypsin and counted. Data are expressed as the mean ± SE of three independent experiments.

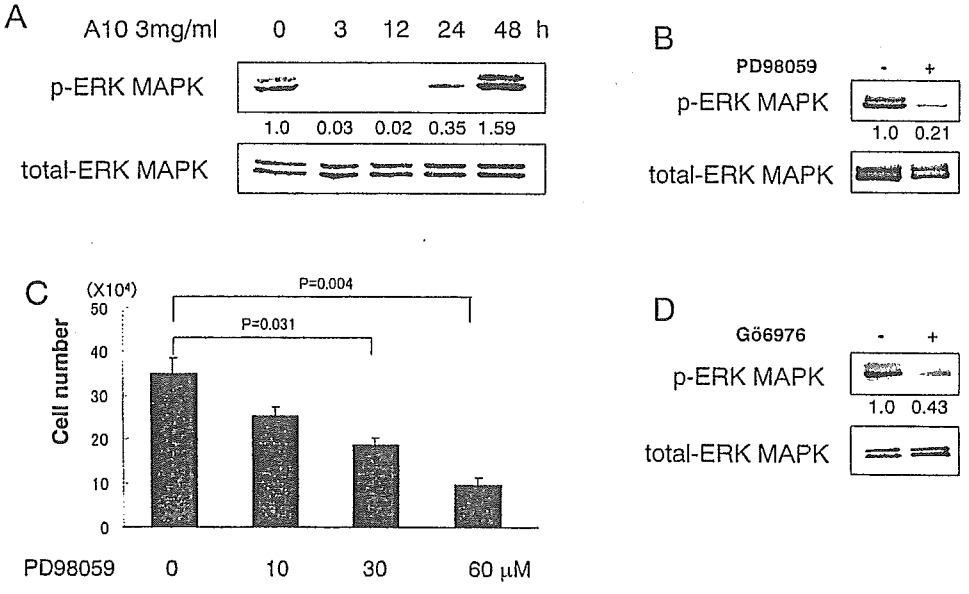

Figure 5. Effect of A10 on ERK MAPK phosphorylation. (A) SKBR-3 cells were treated with 3 mg/ml A10 for different times, as indicated in the figure. Phospho- and total ERK MAPK was assessed by Western blotting. Similar results were observed in two additional experiments. Values indicate the density of the band. (B) Effect of PD98059 on ERK MAPK phosphorylation. Cells were treated with PD98059 (30 μM), and ERK MAPK phosphorylation was assessed 12 h later by Western blotting. Similar results were observed in two additional experiments. Values indicate the density of the band. (C) SKBR-3 cells were treated with different concentrations of PD98059 for 24 h, and the cell number was determined by hemocytometer counting. Data are expressed as the mean ± SE of three independent experiments. (D) Effect of Gö6976 on ERK MAPK phosphorylation. Cells were treated with Gö6976 (3 μM), and ERK MAPK phosphorylation was assessed 12 h later by Western blotting. Similar results were observed in two additional experiments. Values indicate the density of the band.

were suspended by treatment with 0.05% trypsin and counted. Interestingly, Gö6976 produced a significant reduction in the cell number compared to the control (p=0.013). This effect was similar in the presence of A10 (Fig. 4B). Therefore, these results strongly suggest that PKCα is closely involved in the A10-induced inhibition of SKBR-3 cell growth.

Effect of A10 on MAPK. The changes induced by A10 in ERK MAPK were assessed to investigate the pathway downstream from PKC. The addition of A10 produced no change in the total ERK MAPK protein in SKBR-3 cells, but the expression of phosphospecific ERK MAPK decreased markedly 3 h after the 3 mg/ml concentration was added (Fig. 5A). These data suggest that ERK MAPK was closely involved in the A10-induced inhibition of SKBR-3 cell growth. Confirmation of whether ERK MAPK was involved in SKBR-3 cell growth was obtained by adding PD98059, (an inhibitor of mitogen-activated protein kinase kinase [MEK] 1 which is responsible for ERK MAPK activation), to cell cultures and analyzing any changes in cell growth. The expression of phosphorylated ERK MAPK decreased markedly at 12 h after the administration of PD98059, confirming ERK MAPK phosphorylation inhibition by PD98059 (Fig. 5B). The groups receiving 30 or 60 μM PD98059, showed 46.6 and 72.3% growth inhibition, respectively (compared with the control), indicating significant dose-dependent cell growth inhibition ($p<0.05$) (Fig. 5C). To establish a potential role for PKCα in this process, we assessed the effect of Gö6976 on ERK MAPK phosphorylation. Treatment with Gö6976 inhibited ERK MAPK phosphorylation fully after 12 h (Fig. 5D). These results strongly suggested a role for PKCα in the activation of ERK MAPK by A10.

Discussion

The antineoplaston A10 markedly inhibited the proliferation of the breast cancer cell line, SKBR-3, by causing cell-cycle arrest in the G_1 phase. Our findings are consistent with a previous report that demonstrated that antineoplaston induced G_1 arrest and differentiation of human hepatocellular carcinoma cells (24). The mechanism of G_1 arrest by A10 has been suggested to occur at the level of PKC expression and ERK MAPK phosphorylation, since both are important regulators of G_1/S transition. In fact, the expression of PKCα protein decreased markedly on treatment with A10, while other PKC isozymes remained unchanged. On the basis of these results, it is tempting to speculate that PKC, especially PKCα, is involved in the control of G_1/S transition in SKBR-3 cells, probably through controlling essential regulators of G_1/S progression. We used the classical PKC inhibitor, Gö6976, to further investigate how PKCα is involved in the A10-induced inhibition of SKBR-3 cell growth. Interestingly, Gö6976 impaired cell growth significantly. Inhibition of PKCα function, either by pharmacological inhibition with Gö6976 or by reduced protein expression on treatment with A10, impaired the growth of SKBR-3 cells markedly. The lack of an inhibitory effect caused by Gö6976 in A10-treated cells could be related to the low levels of PKCα present after A10 treatment. This would strongly reinforce the concept that PKC plays a major role in the control of cell proliferation in this cell model.

Next, to demonstrate the presence of a signal downstream from PKC, we analyzed MAPK expression. A10 produced little or no change in the expression of the ERK MAPK protein, but its phosphorylation was inhibited 3 h post exposure. This result suggests that ERK MAPK is closely involved in the A10-induced inhibition of SKBR-3 cell growth. This was also supported by the finding that the ERK MAPK-specific inhibitor, PD98059, inhibited cell growth significantly. Moreover, a PKCα blockade with Gö6976 inhibited ERK MAPK phosphorylation, a clear indication that PKCα is an upstream regulator of ERK MAPK in this cell model. Similar findings have been reported in other cell types (25-27).

Among signals downstream of ERK MAPK, control of the cell cycle is considered most important as it is directly related to the control of cell growth. The G_1 phase of the cell cycle is controlled by the cyclin/cyclin dependent kinase (cdk) complex, or inhibitor of cyclin/cdk complex such as p16 or p21 through phosphorylation of Rb (28,29). We therefore assessed the effect of A10 on the expression of cyclins, p16, p21 proteins, and the phosphorylation of Rb. A10 increased the expression of p16 and p21, and inhibited the phosphorylation of Rb at Ser807/811. We speculate that the precise cause of the A10-induced G_1 arrest of SKBR-3 cells was the inhibition of Rb protein phosphorylation associated with the up-regulation of p16 and p21 protein expression. However, in the present study, A10 did not induce changes in cyclin expression, suggesting that G_1 arrest in these cells might be caused by a reduction of cdk kinase activity or some other unidentified factor.

These data lead us to conclude that the exposure of SKBR-3 breast cancer cells to A10 caused the down-regulation of PKCα protein expression, resulting in inhibition of ERK MAPK phosphorylation, increasing p16 and p21 protein expression, with the resultant inhibition of Rb phosphorylation leading to G_1 arrest. Our data indicate the existence of a pathway in which A10 arrests SKBR-3 cells in the G_1 phase via PKC and MAPK. This is the first report, to our knowledge, describing the relationship between antineoplaston and PKC or MAPK. In conclusion, this study suggests that once the mechanism underlying the antineoplaston antitumor effect is fully elucidated, it may provide an effective therapy for breast cancer patients.

References

1. Burzynski SR: Antineoplastons: biochemical defence against cancer. Physiol Chem Phys 8: 275-279, 1976.
2. Burzynski SR: The present state of antineoplaston research (1). Integr Cancer Ther 3: 47-58, 2004.
3. Tsuda H, Sata M, Kumabe T, Uchida M and Hara H: The preventive effect of antineoplaston AS2-1 on HCC recurrence. Oncol Rep 10: 391-397, 2003.
4. Tsuda H, Sata M, Ijuuin H, Kumabe T, Uchida M, Ogou Y, Akagi Y, Shirouzu K, Hara H and Nakashima Y: A novel strategy for remission induction and maintenance in cancer therapy. Oncol Rep 9: 65-68, 2002.
5. Tsuda H, Sata M, Kumabe T, Hara H, Eriguchi N, Sugita Y and Nagamatsu H: Quick response of advanced cancer to chemo-radiation therapy with antineoplastons. Oncol Rep 5: 597-600, 1998.
6. Kumabe T, Tsuda H, Uchida M, Ogoh Y, Hayabuchi N, Sata M, Nakashima O and Hara H: Antineoplaston treatment for advanced hepatocellular carcinoma. Oncol Rep 5: 1363-1367, 1998.
7. Badria F, Mabed M, El-Awadi M, Abou-Zeid L, Al-Nashar E and Hawas S: Immune modulatory potentials of antineoplaston A-10 in breast cancer patients. Cancer Lett 157: 57-63, 2000.
8. Takai Y, Kishimoto A, Inoue M and Nishizuka Y: Studies on acyclic nucleotide-independent protein kinase and its proenzyme in mammalian tissues. I. Purification and characterization of an active enzyme from bovine cerebellum. J Biol Chem 252: 7603-7609, 1977.
9. Nishizuka Y: The molecular heterogeneity of protein kinase C and its implications for cellular regulation. Nature 334: 661-665, 1984.

10. Nishizuka Y: Intracellular signaling hydrolysis of phospholipids and activation of protein kinase C. Science 258: 607-614, 1992.
11. Nishizuka Y: Protein kinase C and lipid signaling for sustained cellular responses. FASEB J 9: 484-496, 1995.
12. Musashi M: The roll of protein kinase C isoform in cell proliferation and apoptosis. Int J Hematol 72: 12-19, 2000.
13. Akkaraju GR and Basu A: Overexpression of protein kinase C-η attenuates caspase activation and tumor necrosis factor-α-induced cell death. Biochem Biophys Res Commun 279: 103-107, 2000.
14. Basu A: Differential sensitivity of breast cancer cells to tumor necrosis factor-α: involvement of protein kinase C. Biochem Biophys Res Commun 280: 883-891, 2001.
15. Gauthier ML, Torretto C, Ly J, Francescutti V and O'Day DH: Protein kinase Cα negatively regulates cell spreading and motility in MDA-MB-231 human breast cancer cells downstream of epidermal growth factor receptor. Biochem Biophys Res Commun 307: 839-846, 2003.
16. Soh JW, Lee YS and Weinstein IB: Effects of regulatory domains of specific isoforms of protein kinase C on growth control and apoptosis in MCF-7 breast cancer cells. J Exp Ther Oncol 3: 115-126, 2003.
17. Shtutman M, Hershko T, Maissel A, Fima E and Livneh E: PKCη associates with cyclin E/Cdk2 complex in serum-starved MCF-7 and NIH-3T3 cells. Exp Cell Res 286: 22-29, 2003.
18. Mao M, Fang X, Lu Y, Lapushin R, Bast RC Jr and Mills GB: Inhibition of growth-factor-induced phosphorylation and activation of protein kinase B/Akt by atypical protein kinase C in breast cancer cells. Biochem J 2: 475-482, 2000.
19. Cowley S, Paterson H, Kemp P and Marshall CJ: Activation of MAP kinase kinase is necessary and sufficient for PC12 differentiation and for transformation of NIH 3T3 cells. Cell 77: 841-852, 1994.
20. Mansour SJ, Matten WT, Hermann AS, Candia JM, Rong S, Fukasawa K, Vande Woude GF and Ahn NG: Transformation of mammalian cells by constitutively active MAP kinase kinase. Science 265: 966-970, 1994.
21. Keshamouni VG, Mattingly RR and Reddy KB: Mechanism of 17-ß-estradiol-induced Erk1/2 activation in breast cancer cells. A role for HER2 AND PKC-δ. J Biol Chem 277: 22558-22565, 2002.
22. Greco S, Muscella A, Elia MG, Salvatore P, Storelli C, Mazzotta A, Manca C and Marsigliante S: Angiotensin II activates extracellular signal regulated kinases via protein kinase C and epidermal growth factor receptor in breast cancer cells. J Cell Physiol 196: 370-377, 2003.
23. Le XF, Marcelli M, McWatters A, Nan B, Mills GB, O'Brian CA and Bast RC Jr: Heregulin-induced apoptosis is mediated by down-regulation of Bcl-2 and activation of caspase-7 and is potentiated by impairment of protein kinase C α activity. Oncogene 20: 8258-8269, 2001.
24. Tsuda H, Iemura A, Sata M, Uchida M, Yamana K and Hara H: Inhibitory effect of antineoplaston A10 and AS2-1 on human hepatocellular carcinoma. Kurume Med J 43: 137-147, 1996.
25. Schonwasser DC, Marais RM, Marshall CJ and Parker PJ: Activation of the mitogen-activated protein kinase/extracellular signal-regulated kinase pathway by conventional, novel and atypical protein kinase C isotypes. Mol Cell Biol 18: 790-798, 1998.
26. Yoon YM, Oh CD, Kim DY, Lee YS, Park JW, Huh TL, Kang SS and Chun JS: Epidermal growth factor negatively regulates chondrogenesis of mesenchymal cells by modulating the protein kinase C-α, Erk-1 and p38 MAPK signaling pathways. J Biol Chem 275: 12353-12359, 2000.
27. Lo LW, Cheng JJ, Chiu JJ, Wung BS, Liu YC and Wang DL: Endothelial exposure to hypoxia induces Egr-1 expression involving PKC α-mediated Ras/Raf-1/ERK1/2 pathway. J Cell Physiol 188: 304-312, 2001.
28. Meyerson M and Harlow E: Identification of G1 kinase activity for cdk6, a novel cyclin D partner. Mol Cell Biol 14: 2077-2086, 1994.
29. Draetta G: Cell cycle control in eukaryotes: molecular mechanisms of cdc2 activation. Trends Biochem Sci 15: 378-383, 1990.

0022-3565/05/3152-888–895$20.00
THE JOURNAL OF PHARMACOLOGY AND EXPERIMENTAL THERAPEUTICS
Copyright © 2005 by The American Society for Pharmacology and Experimental Therapeutics
JPET 315:888–895, 2005

Vol. 315, No. 2
86827/3057515
Printed in U.S.A.

Functional Analysis of Organic Cation Transporter 3 Expressed in Human Placenta

Ryoko Sata, Hisakazu Ohtani, Masayuki Tsujimoto, Hideyasu Murakami, Noriko Koyabu, Takanori Nakamura, Takeshi Uchiumi, Michihiko Kuwano, Hideaki Nagata, Kiyomi Tsukimori, Hitoo Nakano, and Yasufumi Sawada

Department of Medico-Pharmaceutical Sciences (R.S., H.O., M.T., H.M., N.K., Y.S.), Graduate School of Pharmaceutical Sciences, Kyushu University, Fukuoka, Japan; and Departments of Biochemistry (T.N., T.U., M.K.) and Reproduction and Gynecology (H.Nag., K.T., H.Nak.), Graduate School of Medical Sciences, Kyushu University, Fukuoka, Japan

Received March 23, 2005; accepted August 2, 2005

ABSTRACT

The aim of this study is to investigate the placental transport mechanism of cationic compounds by comparison of the uptake of an organic cation into human placental basal membrane vesicles (BLMVs) with that into organic cation transporter 3 (OCT3)-expressing cells. Reverse transcription-polymerase chain reaction analysis demonstrated that OCT3 is the only OCT isoform expressed in the human placenta. The function of OCT3 was investigated by measuring the uptake of 1-methyl-4-phenylpyridinium (MPP^+) into human embryonic kidney (HEK)293 cells stably expressing OCT3 (HEK/OCT3 cells). The OCT3-mediated uptake of MPP^+ was sodium- and chloride-independent and saturable, with a Michaelis constant (K_m) of 82.5 μM. The OCT3-mediated uptake was inhibited by various cationic drugs in a concentration-dependent manner but not by anionic compounds, such as *p*-aminohippuric acid and captopril, or a zwitterion, carnitine. Western blotting analysis of membrane vesicles prepared from human term placenta revealed that OCT3 is expressed only in BLMVs but not in microvillous membrane vesicles. The uptake of MPP^+ into BLMVs was membrane potential-dependent and saturable, with a K_m value of 51.8 μM, which is similar to that in HEK293/OCT3 cells. The inhibitory spectrum of various compounds on MPP^+ uptake by BLMVs was also similar to that in HEK293/OCT3 cells. These results suggest that OCT3 is expressed on the basal membrane of human trophoblast cells and plays an important role in the placental transport of cationic compounds.

Throughout gestation, the placenta plays an important role in regulating the supply of nutrients to the fetus, excretion of metabolic waste products from the fetus, and so on. In the placenta, trophoblast cells, which face the maternal blood, are considered to be the functional entity of the blood-placental barrier. Various transporters have been identified on both microvillous membrane and basal membrane, which face the maternal and fetal side, respectively, of trophoblast cells and are considered to regulate the exchange of various materials between mother and fetus.

Monoamines, including serotonin and norepinephrine, and cationic drugs, such as cimetidine and procainamide, are transported by organic cation transport systems in the kidney and liver (Koepsell, 1998; Kamisako et al., 1999; Dresser et al., 2000; Hohage and Gerhardt, 2000; Suzuki and Sugiyama, 2000). Rat organic cation transporter 1 (rOCT1) was first cloned from rat kidney as a component of the organic cation transport system (Gründemann et al., 1994). Whereas mouse and rat OCT1 are expressed in both liver and kidney (Gründemann et al., 1994; Schweifer and Barlow, 1996), hOCT1 is mainly expressed in the liver (Gorboulev et al., 1997; Zhang et al., 1999). It has also been shown by immunohistochemical study that rOCT1 is expressed on the sinusoidal membrane of hepatocytes (Meyer-Wentrup et al., 1998) and the basolateral membrane of renal tubular epithelium (Karbach et al., 2000; Sugawara-Yokoo et al., 2000).

rOCT2 was cloned as a homolog of rOCT1 from rat kidney (Okuda et al., 1996). Unlike hOCT1, OCT2 is expressed predominantly in the kidney (Okuda et al., 1996; Gorboulev et al., 1997) and is localized on the basolateral membrane of

This study was supported in part by a Grant-in-aid for Young Scientists (A) from the Ministry of Education, Culture, Sports, Science and Technology of Japan.

Article, publication date, and citation information can be found at http://jpet.aspetjournals.org.

doi:10.1124/jpet.105.086827.

ABBREVIATIONS: rOCT, rat organic cation transporter; OCT, organic cation transporter; hOCT, human organic cation transporter; BLMV, human placental basolateral membrane vesicle; MPP^+, 1-methyl-4-phenylpyridinium; RT-PCR, reverse transcription-polymerase chain reaction; HEK, human embryonic kidney; BBMV, human placental microvillous membrane vesicle; PBS, phosphate-buffered saline; ALP, alkaline phosphatase; ANOVA, analysis of variance; PAH, *p*-aminohippuric acid.

renal proximal tubules (Karbach et al., 2000; Sugawara-Yokoo et al., 2000).

Organic cation transporter 3 (OCT3) was first cloned from rat placenta (Kekuda et al., 1998), and its orthologues were also cloned from humans and mice (Gründemann et al., 1998; Verhaagh et al., 1999). Because hOCT3 has high affinity for monoamines, such as histamine, it is also designated as extraneuronal monoamine transporter (Gründemann et al., 1998). In contrast to OCT1 and 2, OCT3 is widely expressed (Kekuda et al., 1998; Verhaagh et al., 1999), although its expression is particularly high in the placenta (Verhaagh et al., 1999). Recently, it has been reported that pregnant OCT3-knockout mice exhibit reduced accumulation of MPP^+ in the embryo compared with pregnant control mice, although the MPP^+ concentration in placenta and amniotic fluid was not affected, suggesting that OCT3 mediates the transport of MPP^+ from the placenta to the fetus but not from the maternal circulation (Zwart et al., 2001). These findings emphasize the importance of OCT3 in the placental transfer of cationic compounds, although its subcellular localization in the placenta and other tissues still remains unknown.

Besides OCTs, various transporters of organic cations have been identified in the human placenta. The expression of OCTN1, a member of a new subfamily of OCTs, has been reported in the human placenta, but its subcellular localization remains to be identified (Tamai et al., 1997). Another OCTN, OCTN2, has been demonstrated to be expressed on the maternal side (microvillous membrane) of trophoblast cells by Western blotting (Lahjouji et al., 2004). An organic cation/proton antiporter, norepinephrine transporter, serotonin transporter, and P-glycoprotein have been found on the microvillous membrane of trophoblast cells (Ganapathy et al., 2000; Ushigome et al., 2003), but the identity of the transporter of organic cations on the basolateral membrane remains unknown. The aim of this study is to investigate the placental transport mechanism of cationic compounds by comparison of the uptake of a model organic cation into human placental basal membrane vesicles (BLMVs) with that into OCT3-expressing cells.

Materials and Methods

Materials and Reagents. [^{3}H]MPP^+ (85.0 Ci/mmol), [^{3}H]quinine (14.5 Ci/mmol), and [^{3}H]dihydroalprenolol (60 Ci/mmol) were purchased from American Radiolabeled Chemicals (St. Louis, MO). [^{14}C]Tetraethylammonium (2.4 Ci/mmol) was purchased from PerkinElmer Life and Analytical Sciences (Boston, MA). [^{3}H]Theophylline (18.5 Ci/mmol) was purchased from Moravek Biochemicals (Brea, CA). Anti-OCT3 goat polyclonal antibody OCT3 (C-14) was purchased from Santa Cruz Biotechnology, Inc. (Santa Cruz, CA). Horseradish peroxidase-labeled anti-goat IgG antibody was purchased from Valeant Pharmaceuticals (Costa Mesa, CA). All other chemicals used in this study were commercial products of reagent grade.

Functional Expression of OCT3 in Mammalian Cells. Human OCT3 cDNA was obtained from human kidney total RNA by RT-PCR using KOD-plus-polymerase (Toyobo Engineering, Osaka, Japan). Sequence analysis revealed that the obtained OCT3 cDNA was 300 base pairs shorter than the OCT3 cloned previously (GenBank accession no. AJ001417; Gründemann et al., 1998). The missing part of the OCT3 cDNA was obtained by PCR using an Advantage-GC Genomic PCR kit (BD Biosciences Clontech, Palo Alto, CA) and human liver cDNA (BD Biosciences Clontech) under the following conditions: 1) 94°C × 3 min; 2) 94°C × 30 s, 68°C × 3 min (35 cycles); and 3) 68°C × 3 min. The full-length OCT3 cDNA was generated using the restriction enzyme BglII and subcloned into pIRESneo vector.

Sequencing of the cDNA was carried out with an ABI Prism BigDye Terminator Cycle Sequencing kit and 373 DNA sequencer (Applied Biosystems, Foster City, CA), and the sequence was analyzed by Sequencing Analysis 3.0 (Applied Biosystems). Sequence analysis showed that there was a G1260A mutation compared with the sequence already published by Gründemann et al. (1998), but it was a silent mutation.

An aliquot of 1 μg of OCT3/pIRESneo vector was transfected into HEK293 cells with LipofectAMINE 2000 Reagent (Invitrogen, Tokyo, Japan). After incubation for 24 h, cells were released by trypsin treatment and cultured in minimal essential medium containing 500 μg/ml geneticin. The cells were grown for 3 to 4 weeks and then used as HEK293 cells stably expressing OCT3 (HEK/OCT3 cells).

Preparation of Human Placental BLMVs and Microvillous Membrane Vesicles (BBMVs). Human placental BLMVs were prepared by the method of Inuyama et al. (2002) with minor modifications. Human term placentas from uncomplicated pregnancies were obtained within 15 min after vaginal or cesarean delivery and placed in 0.9% NaCl. After removal of the cord, amniochorion, and decidua, placental tissue was cut from the maternal side and washed in phosphate-buffered saline (PBS) (−). Tissue was stirred in PBS (−) for 30 min and collected on a nylon mesh. The filtrate was washed three times with ice-cold 50 mM Tris-HCl, pH 7.4, collected on a 250-μm pore size nylon mesh, and divided into several equal portions. Each portion was sonicated in 100 ml of the same Tris buffer using a 3/4-inch-high gain probe for 10 s at 240 W (Vibra-cell; Sonics and Materials, Newtown, CT). The suspensions were kept on ice. The sonication procedure selectively removes any remaining microvillous membrane. Sonicated tissue was collected on the mesh, washed three times with 5 mM Tris-HCl, pH 7.4, and then stirred gently for 60 min in the same buffer. Tissue was then collected on the nylon mesh and washed again in the same buffer. This procedure disrupts and removes the intracellular components, thus exposing the basolateral membranes. Tissue portions of 25 to 30 g were resuspended in approximately 100 ml of 50 mM Tris-HCl, pH 7.4, containing 10 mM EDTA and 250 mM sucrose and incubated for 30 min with occasional stirring. The portions were then sonicated twice for 20 s at 250 W to release the basolateral membranes. The suspensions were strained through nylon mesh, and the supernatant was centrifuged at 3430*g* for 10 min to remove debris. The supernatant from this spin was recentrifuged at 80,000*g* for 40 min to yield the basolateral membrane pellet, which was resuspended, using a Dounce homogenizer in 25 mM HEPES-Tris, pH 7.4, containing 1 mM EDTA and 275 mM sucrose. This fraction was further purified by centrifugation on a discontinuous gradient of 10% (w/v) Ficoll (Pfizer, Inc., New York, NY) in the resuspension buffer overlaid with 4% Ficoll (as described by Kelley et al., 1983) prepared in 25 mM HEPES-Tris, pH 7.4, containing 1 mM EDTA and 275 mM sucrose. Ficoll gradient tubes were spun at 90,000*g* for 6 to 8 h. The material at the density gradient interfaces was collected, washed, and resuspended in 25 mM HEPES-Tris, pH 7.4, containing 275 mM sucrose. The suspension from this run was resuspended in 25 mM HEPES-Tris buffer containing 150 mM KCl, pH 7.4 (E buffer) with a 25-gauge syringe needle. All of the operations were carried out at 4°C.

BBMVs were prepared according to the method described by Nakamura et al. (2002) with minor modifications. Human term placentas from uncomplicated pregnancies were obtained within 15 min after vaginal or cesarean delivery and placed in 0.9% NaCl. After removal of the cord, amniochorion, and decidua, placental tissue was cut from the maternal side and washed in 250 mM mannitol, 10 mM HEPES-Tris at pH 7.4 (MHT buffer). The mince was stirred for 1 h to loosen the microvilli and filtered through two layers of woven cotton gauze. A sample of this starting mince was taken for enzyme analysis. The filtrate was centrifuged at 800*g* for 10 min. The pellet

was discarded, and $MgCl_2$ was added to the supernatant to a final concentration of 10 mM. After 10 min, with occasional stirring, the supernatant was centrifuged at 10,500*g* for 10 min. The pellet was discarded, and the supernatant was centrifuged at 20,000*g* for 20 min. The pellet from this run was suspended in E buffer with a 25-gauge syringe needle. All of the subsequent procedures were performed at 4°C. BLMVs and BBMVs were quickly frozen and stored at −80°C and used within a month.

Tissue homogenate was prepared by the method previously described by Kelley et al. (1983). Approximately 3 g of whole villous tissue was homogenized in 10 ml of buffer E using a Waring blender (PHYSCOTRON Micro Teq.; Nichion Co., Chiba, Japan) for 2.25 min and further with a homogenizer for eight strokes. The material was filtered through six layers of gauze.

Binding activity of [^{3}H]dihydroalprenolol as a marker of the basal membrane and alkaline phosphatase (ALP) activity as a marker of the microvillous membrane was assayed as reported by Kelley et al. (1983) and Bessey et al. (1946), respectively. The dihydroalprenolol binding of BLMVs was 25.2-fold higher than that of the homogenate, whereas the ALP activity was only 3.07-fold higher. On the other hand, the dihydroalprenolol binding of BBMVs was only 1.07-fold higher than that of the homogenate, whereas the ALP activity was 18.3-fold higher. The amount of protein in the sample was measured by the method of Lowry et al. (1951).

RT-PCR Analysis of OCTs mRNA in Human Placenta and BeWo Cells. The total RNAs of BeWo cells and human placenta were extracted with an RNeasy mini kit (QIAGEN GmbH, Hilden, Germany). Human liver total RNA was purchased from Cell Applications, Inc. (San Diego, CA), and human kidney total RNA was purchased form Stratagene (La Jolla, CA). First-strand cDNA was synthesized from total RNA (50 μg), using random primer and SuperScript II reverse transcriptase (Invitrogen, Carlsbad, CA). PCR was performed with a T-Gradient Thermoblock (Biometra, Göttingen, Germany) using KOD-plus-polymerase (Toyobo Engineering) and primers specific for each family member. Table 1 shows the primer sets used in RT-PCR and the accession number of each transporter.

Western Blotting. HEK293/OCT3 cells, BLMVs, and BBMVs were collected and suspended in lysis buffer containing 100 mM Tris-HCl, pH 7.6, 150 mM NaCl, 1 mM $CaCl_2$, 1% Triton X-100, 0.1% SDS, 0.1% Nonidet P-40, 1 mM phenylmethylsulfonyl fluoride, 0.01 mg/ml leupeptin, 0.01 mg/ml aprotinin, and 1 mM sodium vanadate and incubated for 30 to 45 min at 4°C. After incubation, the suspension was centrifuged at 15,000*g* for 15 min at 4°C. SDS-polyacrylamide gel electrophoresis was performed according to the method of Laemmli (1970). The proteins were transferred electrophoretically onto a 0.2-μm pore size Clear Blot Membrane-P (Atto Corporation, Tokyo, Japan). Blots were blocked overnight at 4°C with 5% nonfat powdered milk in PBS (−). OCT3 (C-14) was used as the primary antibody for OCT3, and horseradish peroxidase anti-goat IgG (Valeant Pharmaceuticals) was used as the secondary antibody. Detection was done with enhanced chemiluminescence reagents (GE Healthcare, Little Chalfont, Buckinghamshire, UK) according to the instructions of the manufacturer.

Uptake Experiment into HEK/OCT3 Cells. HEK/OCT3 cells were seeded at 5×10^4 cells/well on 96-well plates (NUNC A/S, Roskilde, Denmark) and grown for 2 days until used for the uptake study.

After reaching confluence, cells were washed twice with uptake buffer (125 mM NaCl, 4.8 mM KCl, 5.6 mM D-glucose, 1.2 mM KH_2PO_4, 1.2 mM $MgSO_4$, and 25 mM HEPES, pH 7.4) before the study. Uptake was initiated by adding 100 μl of uptake buffer containing unlabeled MPP^+ and 10 nM [^{3}H]MPP^+. For the Na^+ dependence study, NaCl was replaced with LiCl, mannitol, or sodium gluconate. After incubation at 37°C for an appropriate time, uptake was terminated by aspiration of the buffer followed by two washes with 1 ml of ice-cold uptake buffer. Cells were then dissolved in 150 μl of 1 N NaOH, and the solution was neutralized with 150 μl of 1 N HCl. Scintillation cocktail (Clear-sol I; Nacalai Tesque, Kyoto, Japan) was added, and the radioactivity of [^{3}H]MPP^+ was determined with a liquid scintillation counter (LS6500; Beckman Coulter, Fullerton, CA). The amount of protein in the cells was measured by the method of Lowry et al. (1951).

Measurement of Uptake into BLMVs and BBMVs. The uptake of [^{3}H]MPP^+ into membrane vesicles was measured by using a rapid filtration technique (Russel et al., 1988). Uptake was initiated by the addition of 90 μl of incubation buffer to 10 μl of BLMV suspension containing 40 to 50 μg of protein. The incubation buffer consisted, in general, of unlabeled MPP^+, 25 mM HEPES-Tris, pH 7.4, 150 mM NaCl, and [^{3}H]MPP^+ (0.08 μCi/point).

At the designated time, uptake was terminated by adding 1 ml of ice-cold stop buffer followed immediately by filtration (HAWP 0.45 μm; Millipore Corporation, Billerica, MA). The filter was washed twice with 4 ml of ice-cold stop buffer. In general, stop buffer contained 10 mM sucrose in incubation buffer. Nonspecific binding was determined by adding 1 ml of ice-cold stop solution and 90 μl of ice-cold incubation buffer to the ice-cold BLMV suspension followed by the same treatment as in the uptake experiments.

To assay radiolabeled compounds, filters were placed in counting vials and mixed with 4 ml of scintillation fluid, Clear-sol I. Radioactivity was measured with a liquid scintillation counter (LS6500).

Data Analysis. The [^{3}H]MPP^+ uptake into HEK/OCT3 cells is expressed as the cell-to-medium ratio calculated from the intracellular uptake per milligram of protein (disintegrations per minute per milligram of protein) of the cells relative to the initial drug concentration (disintegrations per minute per microliter).

As for the uptake into membrane vesicles, obtained radioactivity was normalized with respect to the protein amount of vesicles. Values were determined by subtracting nonspecific binding from total uptake (in the investigation of osmolarity effects as well), and data are presented as the vesicle-to-medium ratio (microliters per milligram of protein).

To determine the kinetic parameters, K_t, J_{max}, and k_d, the following Michaelis-Menten equation was fitted to the data using the nonlinear least-squares regression analysis program MULTI (Yamaoka et al., 1981): $J = J_{max} \times S/(K_t + S) + k_d \times S$, where J and S represent the transport rate and concentration of substrate, respectively. J_{max} (nanomoles per milligram of protein per 30 s), K_t (millimolar), and k_d (microliters per milligram of protein per 30 s) represent the maximum uptake rate for a carrier-mediated process, the Michaelis constant, and the rate constant for the nonsaturable component, respectively.

TABLE 1

Oligonucleotides used for RT-PCR

Open reading frame positions of OCT1, 2, and 3 are 1–1665, 1–1668, and 1–1671, respectively.

Family Member		Sequence	Position	Accession No.
OCT1	Forward	5′-ACTCCGCTCTGGTCGAAATC-3′	1142→1161	X98332
	Reverse	5′-CGACATCGCCGCAAAACATC-3′	1670←1689	
OCT2	Forward	5′-ACTCTGCCCTGGTTGAATTC-3′	1145→1164	X98333
	Reverse	5′-GCAACGGTCTCTCTTCTTAG-3′	1665←1684	
OCT3	Forward	5′-CAGAGATCACTGTTACAGAT-3′	971→990	AJ001417
	Reverse	5′-GATAGCTCCTTCTTTCTGTC-3′	1685←1704	

Comparisons between two and among more than three groups were performed with the unpaired Student's t test and with nonrepeated analysis of variance (ANOVA) followed by Dunnett's test, respectively. The Spearman rank correlation test was used to determine the degree of association between the inhibitory effects on MPP^+ uptake into HEK/OCT3 cells and BLMVs. A P value of less than 0.05 was considered statistically significant.

Results

Expression of OCT mRNAs in Human Placenta and BeWo Cells. The expression of OCTs in human placenta and BeWo cells was examined by RT-PCR analysis. Total RNAs from human liver and kidney were used as positive controls for OCT1 and OCT2 and 3, respectively. In placenta, only OCT3 and the positive control were detected (Fig. 1). The PCR product was confirmed to be in accord with the sequence of human OCT3. With regard to BeWo cells, no band was detected, suggesting that OCTs are not expressed in these cells.

Expression of OCT3 Protein in HEK/OCT3 Cells and Human Placenta. The expression of OCT3 was examined by Western blotting analysis of HEK/OCT3 cells and mock cells (HEK293 cells transfected with vector alone). As expected, a band of 70 kDa was detected only in HEK/OCT3 cells (Fig. 2A).

The expression of OCT3 on human placental trophoblast membrane was also examined by Western blotting analysis using BLMVs and BBMVs prepared from human placenta. The band corresponding to OCT3 was detected in BLMVs at about 70 kDa, as well as in HEK/OCT3 cells, but not in BBMVs (Fig. 2B).

Time Course of the Uptake of MPP^+. The uptake of 1 μM MPP^+ into HEK293/OCT3 cells was significantly higher than that into mock cells (Fig. 3). This uptake was linear for at least 2 min and was attenuated at 4°C. In the following experiments, the initial uptake rate was determined at 30 s.

Effects of Extracellular Ion Composition on the Uptake of MPP^+. The effects of Na^+ and Cl^- on the uptake of MPP^+ were examined by isoosmotic replacement of NaCl (Na^+, +; Cl^-, +) with mannitol (Na^+, −; Cl^-, −), sodium gluconate (Na^+, +; Cl^-, −), and LiCl (Na^+, −; Cl^-, +) in the uptake buffer. As shown in Fig. 4, the uptake of MPP^+ was not affected by any replacement of NaCl, suggesting that OCT3-mediated uptake of MPP^+ is independent of both Na^+ and Cl^-.

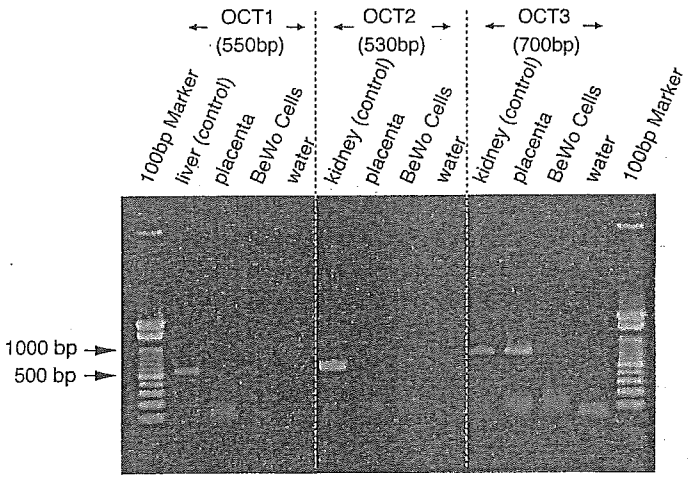

Fig. 1. RT-PCR analysis of the distribution of OCT mRNAs in the human placenta and BeWo cells. Total RNAs from the placenta, liver, kidney, and BeWo cells were reverse-transcribed and used for PCR amplification with oligonucleotide primers specific for OCT1, 2, and 3.

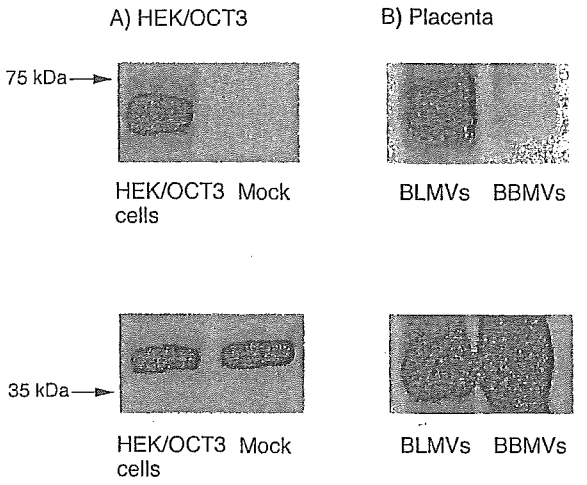

Fig. 2. Western blotting analysis of OCT3 in HEK/OCT3 cells and human placenta. Ten micrograms each of HEK/OCT3 cells and mock (A) and 50 μg each of BLMVs and BBMVs (B) were resolved by SDS-polyacrylamide gel electrophoresis with a 10% polyacrylamide gel and transferred onto Clear Blot Membrane-P. Immunoblots were performed with OCT3-C-14 and anti-β-actin mouse monoclonal antibody and developed with the enhanced chemiluminescence detection reagent. OCT3 and β-actin were detected at 70 and 40 kDa, respectively.

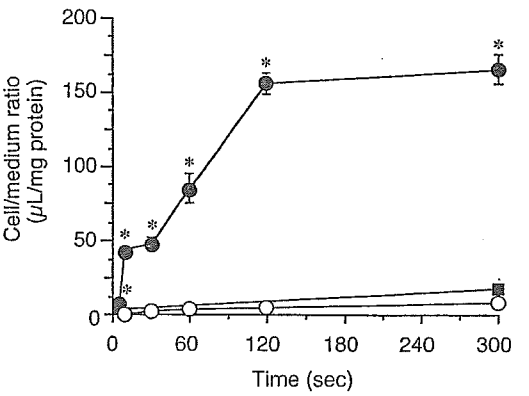

Fig. 3. Time course of OCT3-mediated uptake of 1 μM MPP^+. HEK/OCT3 cells were incubated at 37 (closed circle) and 4°C (closed triangle). HEK293 cells transfected with vector alone (open circle) were incubated at 37°C. Each point represents the mean ± S.E.M. of four determinations. *, $P < 0.05$ versus control (Student's t test).

Concentration-Dependent Uptake of MPP^+. The OCT3-mediated uptake was saturable with a Michaelis constant (K_t) of 82.5 μM (59.7–113.8) [mean (mean − S.D. − mean + S.D.)] and a maximal uptake velocity (J_{max}) of 2538 ± 567.4 pmol/mg protein/30 s (mean ± S.D.) (Fig. 5) obtained from three separate experiments.

Inhibitory Effects of Various Cationic Compounds on the OCT3-Mediated Uptake of MPP^+. The OCT3-mediated uptake of 10 μM MPP^+ was significantly inhibited by various cationic drugs, such as cimetidine, ranitidine, verapamil, quinine, quinidine, imipramine, trimethoprim, and procainamide, in a concentration-dependent manner (Figs. 6 and 7). In contrast, anionic compounds [p-aminohippuric acid (PAH), captopril, and phenobarbital], a zwitterion (carnitine), and a cationic compound (lamivudine) showed little or no inhibitory effect.

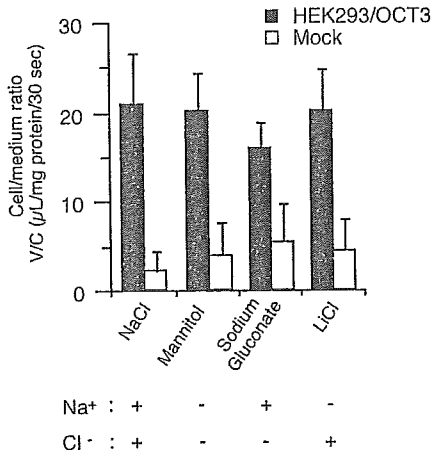

Fig. 4. OCT3-mediated uptake of MPP^+ in the presence or absence of Na^+ or Cl^-. HEK/OCT3 cells were incubated at 37°C for 30 s with 10 μM MPP^+. Uptake buffers of different ionic composition were used: NaCl (Na^+, +; Cl^-, +), mannitol (Na^+, −; Cl^-, −), sodium gluconate (Na^+: +, Cl^-: −), LiCl (Na^+, −; Cl^-, +). Each point represents the mean ± S.E.M. of four determinations.

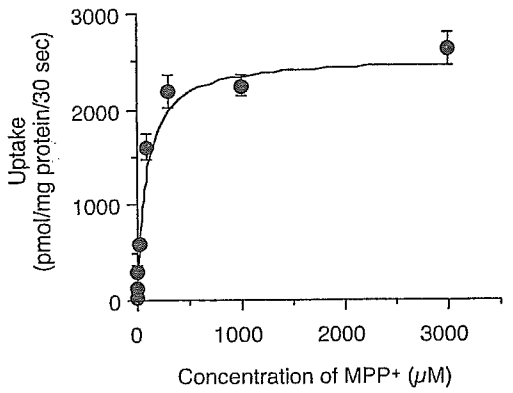

Fig. 5. Concentration-dependent uptake of MPP^+ into HEK/OCT3 cells. Uptake of MPP^+ into HEK/OCT3 cells and mock was measured at concentrations between 1 μM and 3 mM. Data are presented as the OCT3-specific uptake calculated by subtracting the uptake obtained with mock from that obtained with HEK/OCT3. Each point represents the mean ± S.E.M. obtained from three different experiments.

Uptake of Various Cationic Compounds. To search for novel substrates of OCT3, we examined the uptake of 10 μM tetraethylammonium, quinine, theophylline, and ramosetron into HEK/OCT3 cells. No OCT3-mediated uptake of these compounds was observed (data not shown).

Uptake of MPP^+ into BLMVs. The vesicle-to-medium ratio of MPP^+ in BLMVs was linear for at least 30 s (Fig. 8). The vesicle-to-medium ratio at 10 min was reduced with increasing extracellular osmolarity, suggesting that MPP^+ was not only bound to the vesicles but also was taken up into the vesicles.

This uptake was significantly attenuated by replacing extravesicular NaCl with KCl and was potentiated by the addition of valinomycin, a potassium ionophore. The uptake of MPP^+ was not affected by the replacement of NaCl with LiCl (Fig. 9). These results suggested that the uptake of MPP^+ into BLMVs is dependent on membrane potential and independent of Na^+.

Concentration-Dependent Uptake of MPP^+ into BLMVs. The uptake of MPP^+ into BLMVs was saturable with a Michaelis constant (K_t) of 51.8 μM [34.9–113.8] (mean [mean − S.D. − mean + S.D.]) and a maximal uptake velocity (J_{max}) of 332 ± 30.8 pmol/mg protein/30 s (mean ± S.D.) (Fig. 10) obtained from three separate experiments.

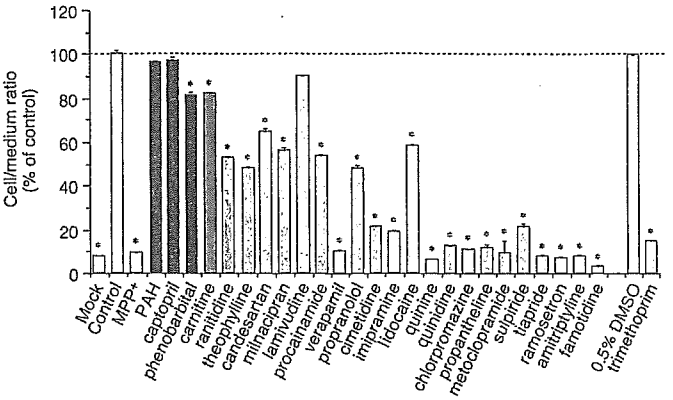

Fig. 6. Inhibitory effects of several drugs on the uptake of MPP^+ into HEK/OCT3 cells. HEK/OCT3 cells were incubated at 37°C for 30 s with 10 μM MPP^+ in the absence or presence of 1 mM various compounds. Results are given as percentage of control uptake measured in the absence of inhibitors. The control and control [+0.5% dimethyl sulfoxide (DMSO)] values were 27.38 and 25.04 μl/mg protein/30 s. Each point represents the mean ± S.E.M. of four determinations. *, $P < 0.05$ versus respective control (ANOVA; Dunnett's test).

Effects of Various Compounds on the Uptake of MPP^+ into BLMVs. We examined the effects of various compounds of the uptake of MPP^+ into BLMVs. We selected noninhibitors (PAH, captopril, and lamivudin), modest inhibitors (carnitine and procainamide), and strong inhibitors (cimetidine, imipramine, quinidine, verapamil, and quinine) of OCT3-mediated uptake. As shown in Fig. 11, PAH and procainamide showed little or no inhibitory effect, whereas quinine, quinidine, imipramine, and verapamil inhibited the uptake of MPP^+ into BLMVs. The rank order of the inhibitory effects of MPP^+ uptake into HEK/OCT3 cells was highly correlated with that in BLMVs ($r^2 = 0.688$, $P < 0.05$; Fig. 12).

Discussion

To investigate the placental transport mechanism of cationic compounds, we focused on OCTs in this study. Because the only OCT detected in human placenta by RT-PCR analysis was OCT3, this molecule is expected to play an important role in the transport of cationic compounds across the human placenta.

hOCT1 and hOCT2 are predominantly expressed in the liver and kidney, respectively (Gorboulev et al., 1997). Unlike OCT1 and OCT2, OCT3 is widely expressed (Kekuda et al., 1998; Verhaagh et al., 1999). The OCT3 mRNA level in the placenta is particularly high, being 2.5 and 5 times that in the liver and kidney, respectively. OCT3 is considered to be one of the most abundantly expressed transporters in the placenta (Leazer and Klaassen, 2003). Our results are consistent with that finding and underscore the key role of OCT3 in the transport of cationic compounds in the placenta.

We also investigated OCTs in a human choriocarcinoma trophoblast cell line, BeWo cells, and found no expression of OCTs. This finding is in accordance with the results of Wu et al. (2000). Although the BeWo cell line originated from placenta, it has the characteristics of cytotrophoblast cells and is functionally and morphologically distinct from normal syncytiotrophoblast cells (Ugele and Simon, 1999). Thus, it is not surprising that OCT3 is not expressed in BeWo cells.

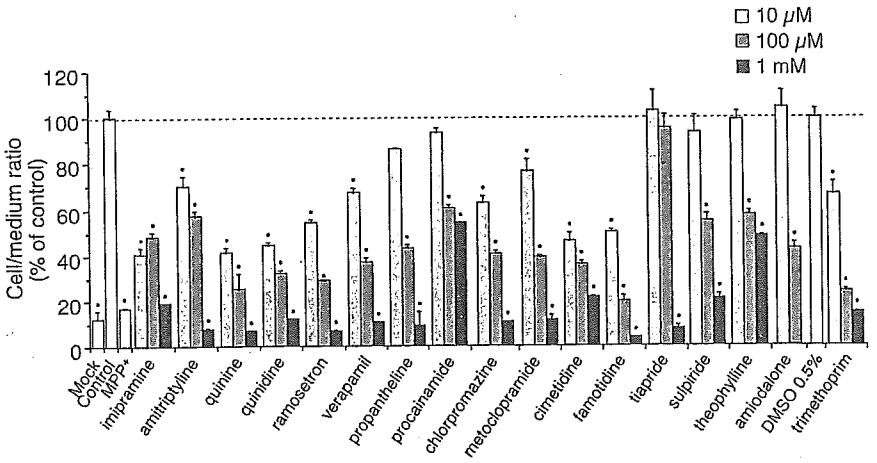

Fig. 7. Inhibitory effects of several drugs on the uptake of MPP^+ into HEK/OCT3 cells. HEK/OCT3 cells were incubated at 37°C for 30 s with 10 μM MPP^+, in the absence or presence of 10 or 100 μM or 1 mM inhibitors. Results are given as percentage of control uptake measured in the absence of inhibitors. The control and control [+0.5% dimethyl sulfoxide (DMSO)] values were 29.97 μl/mg protein/30 s and 28.54 μl/mg protein/30 s. Each point represents the mean ± S.E.M. of four determinations. *, $P < 0.05$ versus respective control (ANOVA; Dunnett's test).

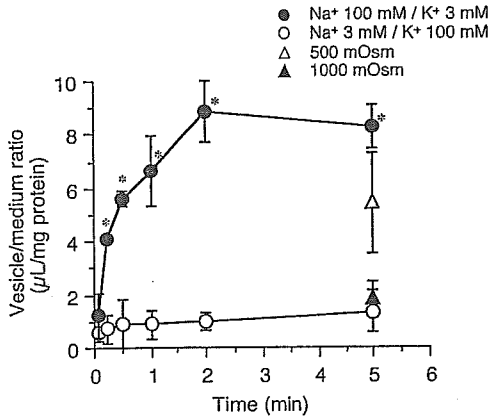

Fig. 8. Influence of Na^+ on the uptake of MPP^+ into BLMVs. Uptake was initiated by the addition of 10 μM MPP^+ in the presence of Na^+ 100 mM/K^+ 3 mM (closed circle) or Na^+ 3 mM/K^+ 100 mM (open circle). Each point represents the mean ± S.E.M. of three determinations. *, $P < 0.05$ versus control (Student's t test).

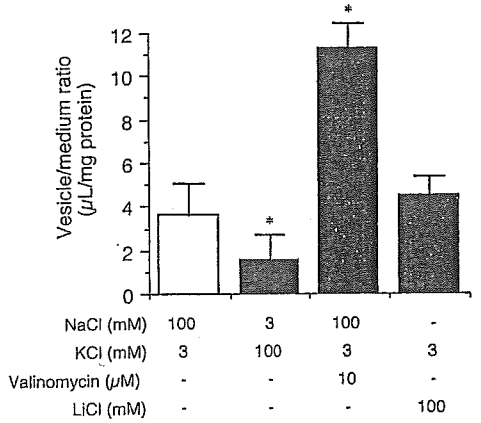

Fig. 9. Influence of membrane potential on the uptake of MPP^+ into BLMVs. Uptake was initiated by the addition of 10 μM MPP^+. Ionic composition of uptake buffers is shown below the figure. Each point represents the mean ± S.E.M. of three determinations. *, $P < 0.05$ versus control (ANOVA; Dunnett's test).

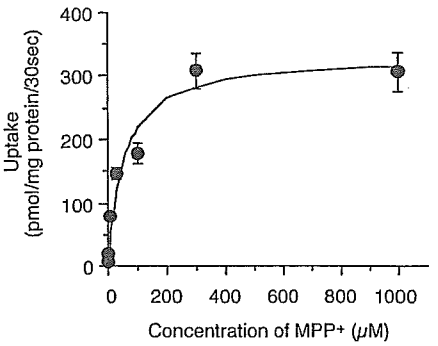

Fig. 10. Concentration-dependent uptake of MPP^+ into BLMVs. Uptake of MPP^+ into BLMVs was measured at concentrations between 1 μM and 1 mM. Uptake was initiated by the addition of 10 μM MPP^+ in the presence of Na^+ 100 mM/K^+ 3 mM. Each point represents the mean ± S.E.M. obtained from three different experiments.

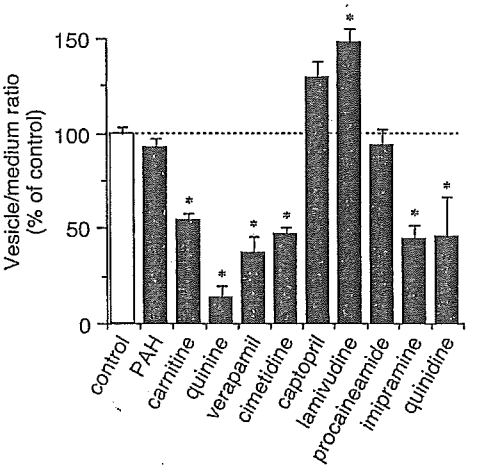

Fig. 11. Inhibitory effects of several drugs on the uptake of 10 μM MPP^+ into BLMVs. BLMVs were incubated at 37°C for 30 s with 10 μM MPP^+, in the absence or presence of 1 mM various compounds. Results are given as percentage of control uptake measured in the absence of inhibitors. The control values were 4.02 μl/mg protein/30 s. Each point represents the mean ± S.E.M. of three determinations. *, $P < 0.05$ versus control (ANOVA; Dunnett's test).

Western blotting demonstrated predominant expression of OCT3 in HEK/OCT3 cells. It was detected as a band of 70 kDa, which is larger than expected from the amino acid sequence (62 kDa) (Fig. 2). Because both mouse and rat OCT3 have four to five N-glycosylation sites (Burckhardt and Wolff, 2000) and hOCT3 shows 90% homology to them, the difference in size is likely to be attributable to glycosylation. Indeed, the size of the bands of OCT3 from both BLMVs and HEK/OCT3 cells was 70 kDa. The established HEK/OCT3 cells transported MPP^+ with a K_t value of 69 μM (Fig. 5), which is in good agreement with the values reported for human retinal pigment epithelial cells (47 μM; Wu et al., 2000) and HEK293 (104 μM; Martel et al., 2001).

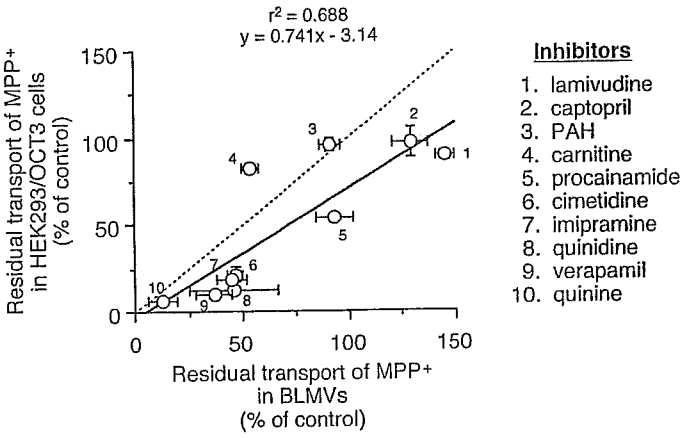

Fig. 12. Comparison of inhibitory effects on MPP^+ uptake between HEK/OCT3 cells and BLMVs. The solid line shows the linear regression and the dashed line shows the 1:1 line. The concentration of each inhibitor was 1 mM. Each point represents the mean ± S.E.M. of three (BLMVs) or four (HEK/OCT3 cells) determinations.

The uptake of MPP^+, a typical substrate of OCT3, into HEK/OCT3 cells was inhibited by cationic compounds, such as cimetidine, verapamil, quinine, quinidine, ramosetron, and trimethoprim, in a concentration-dependent manner. In contrast, anionic compounds, including PAH, captopril, and phenobarbital, and a zwitterion, carnitine, showed little or no inhibitory effect (Figs. 6 and 7). In addition to well known inhibitors of OCT3, such as cimetidine, imipramine, and quinine (Gründemann et al., 1998; Wu et al., 2000), we have identified a variety of cationic drugs that inhibit OCT3. Interestingly, a cationic compound, lamivudine, did not inhibit OCT3 function, suggesting that cationic character alone is not sufficient for recognition by OCT3. Among therapeutic drugs, only cimetidine is known to be a substrate of OCT3 (Gründemann et al., 1999). Because various cationic drugs were found to inhibit OCT3, some of them might be substrates of OCT3.

To search for novel substrates of OCT3, we also examined the uptake of tetraethylammonium, quinine, theophylline, and ramosetron into HEK/OCT3 cells. Although tetraethylammonium is a typical substrate of OCT1 and 2 as well as MPP^+, none of the above-mentioned drugs was a substrate for OCT3. Our finding in the case of tetraethylammonium is consistent with previous reports that the affinity of tetraethylammonium for mouse and rat OCT3 is approximately 10-fold weaker than that for OCT1 and 2 (Kekuda et al., 1998; Wu et al., 2000) and that hOCT3 does not interact with tetraethylammonium (Gründemann et al., 1999). In contrast, OCT3 has high affinity for monoamines (Gründemann et al., 1998). Overall, OCT3 seems to have a substrate specificity distinct from those of OCT1 and 2.

Western blot analysis of BLMVs and BBMVs showed that OCT3 is predominantly expressed on the basolateral membrane of trophoblast cells (Fig. 2). Recently, it has been reported that accumulation of MPP^+ in the embryo was reduced in OCT3-knockout pregnant mice, although MPP^+ concentrations in the placenta and amniotic fluid were comparable (Zwart et al., 2001), suggesting that OCT3 mediates the transport of MPP^+ from the placenta to the fetus but not from the maternal circulation to the placenta. This finding is consistent with our results that OCT3 is expressed on the basolateral membrane of trophoblast cells. Although various transporters, such as organic cation/proton antiporter, norepinephrine transporter, and serotonin transporter, were shown to be localized at the microvillous membrane of placental trophoblast cells (Ganapathy et al., 2000), nothing was known about the expression of transporters for cationic compounds on the basolateral membrane of trophoblast cells. Herein, we have demonstrated for the first time the expression and function of OCT3 on the basal membrane, where it presumably plays a role in the excretion of metabolic waste products or xenobiotics from the fetus. With regard to the transport direction, OCT3 has been considered to transport cationic compounds bidirectionally in a concentration-dependent manner (Kekuda et al., 1998). OCT3 may transport the maternally administered cationic compounds from the placenta to the fetal side and transport oppositely the cationic compounds whose level is higher in the fetal blood.

We compared quantitatively the transport properties of cationic compounds in human placental membrane vesicles with those of HEK/OCT3 cells. The uptake of MPP^+ into BLMVs was membrane potential-sensitive and Na^+-independent (Fig. 9). The K_m values of MPP^+ uptake into BLMVs and HEK/OCT3 cells were similar (39 and 70 μM, respectively). Moreover, the inhibitory effects of various compounds on the uptake of MPP^+ into BLMVs were highly correlated with those on uptake into HEK/OCT3 cells (Fig. 12). Because we did not examine detailed mechanism for the inhibition by drugs, we cannot exclude the possibility that they inhibited OCT3 in a noncompetitive manner by a nonspecific mechanism, such as membrane depolarization and so on. Although the inhibitory mechanism by these compounds remains to be further investigated, the inhibitory nature is unlikely to significantly affect the conclusion that OCT3 plays an important role in the placental transport of cationic compounds.

In summary, we have identified the expression of OCT3 on the basal membranes of trophoblast cells. Because the properties of MPP^+ uptake into BLMVs are similar to those in HEK/OCT3 cells, OCT3 is likely to be predominantly responsible for the transport of cationic compounds across the basolateral membranes of trophoblast cells.

References

Bessey OA, Lowry OH, and Brock MJ (1946) A method of the rapid determination of alkaline phosphatase with five cubic millimeters of serum. *J Biol Chem* 28:321–329.

Burckhardt G and Wolff NA (2000) Structure of renal organic anion and cation transporters. *Am J Physiol* 278:F853–F866.

Dresser MJ, Leabman MK, and Giacomini KM (2000) Transporters involved in the elimination of drugs in the kidney: organic anion transporters and organic cation transporters. *J Pharm Sci* 90:397–421.

Ganapathy V, Prasad PD, Ganapathy ME, and Leibach FH (2000) Placental transporters relevant to drug distribution across the maternal-fetal interface. *J Pharmacol Exp Ther* 294:413–420.

Gorboulev V, Ulzheimer JC, Akhoundova A, Ulzheimer-Teuber I, Karbach U, Quester S, Baumann C, Lang F, Busch AE, and Koepsell H (1997) Cloning and characterization of two human polyspecific organic cation transporters. *DNA Cell Biol* 16:871–881.

Gründemann D, Gorboulev V, Gambaryan S, Veyhl M, and Koepsell H (1994) Drug excretion mediated by a new prototype polyspecific transporter. *Nature (Lond)* 372:549–552.

Gründemann D, Liebich G, Kiefer N, Koster S, and Schomig E (1999) Selective substrates for non-neuronal monoamine transporters. *Mol Pharmacol* 56:1–10.

Gründemann D, Schechinger B, Rappold GA, and Schomig E (1998) Molecular identification of the corticosterone-sensitive extraneuronal catecholamine transporter. *Nat Neurosci* 1:349–351.

Hohage H and Gerhardt U (2000) Inorganic anions and the renal organic cation transport system. *Life Sci* 66:1–9.

Inuyama M, Ushigome F, Emoto A, Koyabu N, Satoh S, Tsukimori K, Nakano H, Ohtani H, and Sawada Y (2002) Characteristics of L-lactic acid transport in basal membrane vesicles of human placental syncytiotrophoblast. *Am J Physiol* 283: C822–C830.

Kamisako T, Gabazza EC, Ishihara T, and Adachi Y (1999) Molecular aspects of

organic compound transport across the plasma membrane of hepatocytes. *J Gastroenterol Hepatol* 14:405–412.
Karbach U, Kricke J, Meyer-Wentrup F, Gorboulev V, Volk C, Loffing-Cueni D, Kaissling B, Bachmann S, and Koespell H (2000) Localization of organic cation transporters OCT1 and OCT2 in rat kidney. *Am J Physiol* 279:F679–F687.
Kekuda R, Prasad PD, Wu X, Wang H, Fei YJ, Leibach FH, and Ganapathy V (1998) Cloning and functional characterization of a potential-sensitive, polyspecific organic cation transporter (OCT3) most abundantly expressed in placenta. *J Biol Chem* 273:15971–15979.
Kelley LK, Smith CH, and King BF (1983) Isolation and partial characterization of the basal cell membrane of human placental trophoblast. *Biochim Biophys Acta* 734:91–98.
Koepsell H (1998) Organic cation transporters in intestine, kidney, liver and brain. *Annu Rev Physiol* 60:243–266.
Laemmli UK (1970) Cleavage of structural proteins during the assembly of the head of bacteriophage T4. *Nature (Lond)* 227:680–685.
Lahjouji K, Elimrani I, Lafond J, Leduc L, Qureshi IA, and Mitchell GA (2004) L-Carnitine transport in human placental brush-border membranes is mediated by the sodium-dependent organic cation transporter OCTN2. *Am J Physiol* 287: C263–C269.
Leazer TM and Klaassen CD (2003) The presence of xenobiotic transporters in the rat placenta. *Drug Metab Dispos* 31:153–167.
Lowry OH, Rosebrough NJ, Farr AL, and Randall RJ (1951) Protein measurement with the Folin phenol reagent. *J Biol Chem* 193:265–275.
Martel F, Keating E, Calhau C, Gründemann D, Schömig E, and Azevedo I (2001) Regulation of human extraneuronal monoamine transporter (hEMT) expressed in HEK293 cells by intracellular second messenger systems. *Naunyn-Schmiedeberg's Arch Pharmacol* 364:487–495.
Meyer-Wentrup F, Karbach U, Gorboulev V, Arndt P, and Koespell H (1998) Membrane localization of the electrogenic cation transporter rOCT1 in rat liver. *Biochem Biophys Res Commun* 248:673–678.
Nakamura H, Ushigome F, Koyabu N, Satoh S, Tsukimori K, Nakano H, Ohtani H, and Sawada Y (2002) Proton gradient-dependent transport of valproic acid in human placental brush-border membrane vesicles. *Pharm Res* 19:154–161.
Okuda M, Saito H, Urakami Y, Takano M, and Inui K (1996) cDNA cloning and functional expression of a novel rat kidney organic cation transporter, OCT2. *Biochem Biophys Res Commun* 224:500–507.
Russel FG, van der Linden PE, Vermeulen WG, Heijn M, van Os CH, and van Ginneken CA (1988) Na^+ and H^+ gradient-dependent transport of *p*-aminohippurate in membrane vesicles from dog kidney cortex. *Biochem Pharmacol* 37:2639–2649.
Schweifer N and Barlow DP (1996) The Lx1 gene maps to mouse chromosome 17 and codes for a protein that is homologous to glucose and polyspecific transmembrane transporters. *Mamm Genome* 7:735–740.
Sugawara-Yokoo M, Urakami Y, Koyama H, Fujikura K, Masuda S, Saito H, Naruse T, Inui K, and Takata K (2000) Differential localization of organic cation transporters rOCT1 and rOCT2 in the basolateral membrane of rat kidney proximal tubules. *Histochem Cell Biol* 114:175–180.
Suzuki H and Sugiyama Y (2000) Transport of drugs across the hepatic sinusoidal membrane: sinusoidal drug influx and efflux in the liver. *Semin Liver Dis* 20:251–263.
Tamai I, Yabuuchi H, Nezu J, Sai Y, Oku A, Shimane M, and Tsuji A (1997) Cloning and characterization of a novel human pH-dependent organic cation transporter, OCTN1. *FEBS Lett* 419:107–111.
Ugele B and Simon S (1999) Uptake of dehydroepiandrosterone-3-sulfate by isolated trophoblasts from human term placenta, JEG-3, BeWo, Jar, BHK cells and BHK cells transfected with human sterylsulfatase-cDNA. *J Steroid Biochem Mol Biol* 71:203–211.
Ushigome F, Koyabu N, Satoh S, Tsukimori K, Nakano H, Nakamura T, Uchiumi T, Kuwano M, Ohtani H, and Sawada Y (2003) Kinetic analysis of P-glycoprotein-mediated transport by using normal human placental brush-border membrane vesicles. *Pharm Res* 20:38–44.
Verhaagh S, Schweifer N, Barlow DP, and Zwart R (1999) Cloning of the mouse and human solute carrier 22a3 (Slc22a3/SLC22A3) identifies a conserved cluster of three organic cation transporters on mouse chromosome 17 and human 6q26–q27. *Genomics* 55:209–218.
Wu X, Huang W, Ganapathy ME, Wang H, Kekuda R, Conway SJ, Leibach FH, and Ganapathy V (2000) Structure, function and regional distribution of the organic cation transporter OCT3 in the kidney. *Am J Physiol* 279:F449–F458.
Yamaoka K, Tanigawara Y, Nakagawa T, and Uno T (1981) A pharmacokinetic analysis program (MULTI) for microcomputer. *J Pharmacobio-Dyn* 4:879–881.
Zhang L, Gorset W, Dresser MJ, and Giacomini KM (1999) The interaction of *n*-tetraalkylammonium compounds with a human organic cation transporter, hOCT1. *J Pharmacol Exp Ther* 288:1192–1198.
Zwart R, Verhaagh S, Buitelaar M, Popp-Snijders C, and Barlow DP (2001) Impaired activity of the extraneuronal monoamine transporter system known as uptake-2 in *Orct3/Slc22a3*-deficient mice. *Mol Cell Biol* 21:4188–4196.

Address correspondence to: Dr. Yasufumi Sawada, Graduate School of Pharmaceutical Sciences, Kyushu University, 3-1-1 Maidashi, Higashi-ku, Fukuoka 812-8582, Japan. E-mail: sawada@phar.kyushu-u.ac.jp